## RESEARCH ARTICLE

*Integrative Cardiovascular Physiology and Pathophysiology*

# Estimating central blood pressure from aortic flow: development and assessment of algorithms

Jorge Mariscal-Harana,[1] Peter H. Charlton,[1] Samuel Vennin,[1,2] Jorge Aramburu,[3] Mateusz Cezary Florkow,[1,4] Arna van Engelen,[1] Torben Schneider,[5] Hubrecht de Bliek,[6] Bram Ruijsink,[1,7] Israel Valverde,[1,8] Philipp Beerbaum,[9] Heynric Grotenhuis,[10] Marietta Charakida,[1] Phil Chowienczyk,[2] Spencer J. Sherwin,[11] and Jordi Alastruey[1,12]

[1]*Department of Biomedical Engineering, School of Biomedical Engineering and Imaging Sciences, King's College London, King's Health Partners, London, United Kingdom;* [2]*Department of Clinical Pharmacology, King's College London, King's Health Partners, London , United Kingdom;* [3]*TECNUN Escuela de Ingenieros, Universidad de Navarra, Donostia-San Sebastián, Spain;* [4]*Philips Research, Cambridge, United Kingdom;* [5]*Philips Healthcare UK, Philips Centre, Guildford Business Park, Guildford, Surrey, United Kingdom;* [6]*HSDP Clinical Platforms, Philips Healthcare, Eindhoven, The Netherlands;* [7]*Department of Cardiology, University Medical Centre Utrecht, Utrecht, The Netherlands;* [8]*Cardiovascular Pathophysiology, Institute of Biomedicine of Seville, University Hospital of Virgen del Rocío, University of Seville, CIBERCV, CSIC, Seville, Spain;* [9]*Department of Pediatric Cardiology and Intensive Care, Hannover Medical School, Hannover, Germany;* [10]*Department of Pediatric Cardiology, University Medical Center Utrecht/Wilhelmina Children's Hospital, Utrecht, The Netherlands;* [11]*Department of Aeronautics, South Kensington Campus, Imperial College London, London, United Kingdom; and* [12]*Institute of Personalized Medicine, Sechenov University, Moscow, Russia*

## Abstract

Central blood pressure (cBP) is a highly prognostic cardiovascular (CV) risk factor whose accurate, invasive assessment is costly and carries risks to patients. We developed and assessed novel algorithms for estimating cBP from noninvasive aortic hemodynamic data and a peripheral blood pressure measurement. These algorithms were created using three blood flow models: the two- and three-element Windkessel (0-D) models and a one-dimensional (1-D) model of the thoracic aorta. We tested new and existing methods for estimating CV parameters (left ventricular ejection time, outflow BP, arterial resistance and compliance, pulse wave velocity, and characteristic impedance) required for the cBP algorithms, using virtual (simulated) subjects ($n$ = 19,646) for which reference CV parameters were known exactly. We then tested the cBP algorithms using virtual subjects ($n$ = 4,064), for which reference cBP were available free of measurement error, and clinical datasets containing invasive ($n$ = 10) and noninvasive ($n$ = 171) reference cBP waves across a wide range of CV conditions. The 1-D algorithm outperformed the 0-D algorithms when the aortic vascular geometry was available, achieving central systolic blood pressure (cSBP) errors $\leq 2.1 \pm 9.7$ mmHg and root-mean-square errors (RMSEs) $\leq 6.4 \pm 2.8$ mmHg against invasive reference cBP waves ($n$ = 10). When the aortic geometry was unavailable, the three-element 0-D algorithm achieved cSBP errors $\leq 6.0 \pm 4.7$ mmHg and RMSEs $\leq 5.9 \pm 2.4$ mmHg against noninvasive reference cBP waves ($n$ = 171), outperforming the two-element 0-D algorithm. All CV parameters were estimated with mean percentage errors $\leq 8.2\%$, except for the aortic characteristic impedance ($\leq 13.4\%$), which affected the three-element 0-D algorithm's performance. The freely available algorithms developed in this work enable fast and accurate calculation of the cBP wave and CV parameters in datasets containing noninvasive ultrasound or magnetic resonance imaging data.

**NEW & NOTEWORTHY** First, our proposed methods for CV parameter estimation and a comprehensive set of methods from the literature were tested using in silico and clinical datasets. Second, optimized algorithms for estimating cBP from aortic flow were developed and tested for a wide range of cBP morphologies, including catheter cBP data. Third, a dataset of simulated cBP waves was created using a three-element Windkessel model. Fourth, the Windkessel model dataset and optimized algorithms are freely available.

*blood flow models; central blood pressure; magnetic resonance imaging; ultrasound; virtual subjects*

## INTRODUCTION

Recent clinical studies have shown that central (aortic) blood pressure (cBP) is a better cardiovascular risk indicator than brachial blood pressure (bBP) (1–4), since cBP is more representative of the load exerted on major organs (1, 5). Regardless of gender or disease, cBPs in subjects with similar brachial systolic blood pressure (SBP) may differ by up to 33 mmHg, resulting in "a significant overlap of central SBP scores between brachial SBP risk groups" (6). Furthermore, bBP can be misleading in healthy young adults due to central-brachial pulse pressure (PP) amplification of up to 30 mmHg (7). The most direct method to measure cBP is cardiac catheterization, which is costly and carries risks to patients (e.g., blood clot formation and embolization) due to its invasive nature, even when performed in specialized centers (2). Consequently, there is great value in developing methods for estimating cBP noninvasively that are less risky and more suitable for frequent use.

A potential approach is to use a computational model of the circulation to estimate cBP from noninvasive measurements of aortic flow and peripheral blood pressure (BP) (8). Aortic flow can be measured using magnetic resonance imaging (MRI) or ultrasound (US). Peripheral systolic and diastolic BP can be easily measured using a brachial cuff, whereas a peripheral BP wave can be measured using, for example, applanation tonometry. MRI can also measure vascular geometry, which can be used to further refine the model—the importance of aortic geometry was proposed by Westerhof et al. (9). Consequently, computational models could be personalized to estimate cBP in cardiac MRI and US settings. Moreover, these imaging modalities are the gold standard when assessing cardiac anatomy (cardiac magnetic resonance and echocardiography). Combining the information they provide with the knowledge of cBP could enable the noninvasive derivation of pressure-volume loops and myocardial wall stress, two major indicators of cardiac performance. Although previous studies have used reduced-order models to estimate cBP noninvasively, they either did not use patient-specific MRI aortic geometry (10) or did not validate their cBP estimates against invasive cBP measurements or compare the performance of several algorithms (8, 11–14).

The aim of this study was to develop and assess three novel algorithms of increasing complexity for estimating the cBP wave from aortic flow, using noninvasive, patient-specific data from the thoracic aorta (Fig. 1). Each algorithm used a different blood flow model: the two-element (15) and three-element (16) zero-dimensional (0-D) Windkessel models and a one-dimensional (1-D) model of the thoracic aorta (11). The first step in each algorithm was to estimate cardiovascular (CV) parameters from noninvasive hemodynamic data measured in the thoracic aorta and a peripheral BP measurement. These CV parameters were left ventricular ejection time (LVET), outflow vascular BP ($P_{out}$), total arterial resistance ($R_T$) and compliance ($C_T$), aortic pulse wave velocity (PWV), and characteristic impedance ($Z_O$). The second step was to use these parameters as inputs to one of the three blood flow models to estimate a patient-specific cBP waveform. In this study, we assessed the performance of the CV parameter estimation methods and cBP algorithms against reference data, including invasive cBP measurements.

## METHODS

### Datasets

The CV parameter estimation methods and cBP algorithms were initially developed and tested using two datasets of virtual subjects. The cBP algorithms were then assessed using three clinical datasets. The characteristics of each dataset are shown in Table 1.

#### *Clinical datasets.*

The first clinical dataset, called the aortic coarctation dataset, contains data acquired from 10 patients with aortic coarctation (17). The St Thomas' Hospital Research Ethics Committee approved this prospective study, and informed consent was obtained from all patients (ethics reference number R&D REC 08/H0804/134). Inclusion criteria comprised native or residual aortic coarctation. Exclusion criteria were the presence of stented aortic coarctation or aortic dissection. Data were acquired in a hybrid magnetic resonance/X-ray suite guidance system. A 1.5-T MRI scanner (Philips Intera, Philips, Best, The Netherlands) was used to obtain a breath-hold three-dimensional contrast-enhanced angiography of the thoracic aorta (used to obtain aortic geometry measurements) and free-breathing two-dimensional phase contrast flow velocity through-plane scans at the ascending and upper-descending aortas (used to obtain flows at both locations). Invasive BP data were measured using X-ray-guided cardiac catheterization (Philips BV Pulsera). Measurements were taken simultaneously at the ascending and descending aortas, immediately after the flow acquisition, using multipurpose catheters (angiographic catheter 4F with carbon dioxide-filled balloon).

The second and third clinical datasets, called the normotensive and hypertensive datasets, were obtained from (18): *1*) 13 normotensive healthy volunteers at baseline and after the administration of different doses of four inotropic and vasoactive drugs (dobutamine, norepinephrine, phentolamine, and nitroglycerin) and *2*) 158 subjects assessed for hypertension (including those found to be normotensive). Both datasets were approved by the London-Westminster Research Ethics Committee, and written informed consent was obtained. Aortic flow was obtained by Doppler sonography, and peripheral BP measurements were obtained by carotid applanation tonometry. Reference cBP measurements were acquired using the SphygmoCor system (AtCor Medical, Sydney, Australia), which uses a transfer function to calculate cBP from carotid BP measured noninvasively by applanation tonometry (1, 19).

The range of cBP waves contained within each clinical dataset is shown in Fig. 2.

#### *Datasets of virtual subjects.*

Two datasets of BP and flow waves measured in virtual subjects were created by simulating arterial hemodynamics using 0-D and 1-D computational models, respectively (Fig. 3). A new 0-D dataset, whose reference CV parameter values
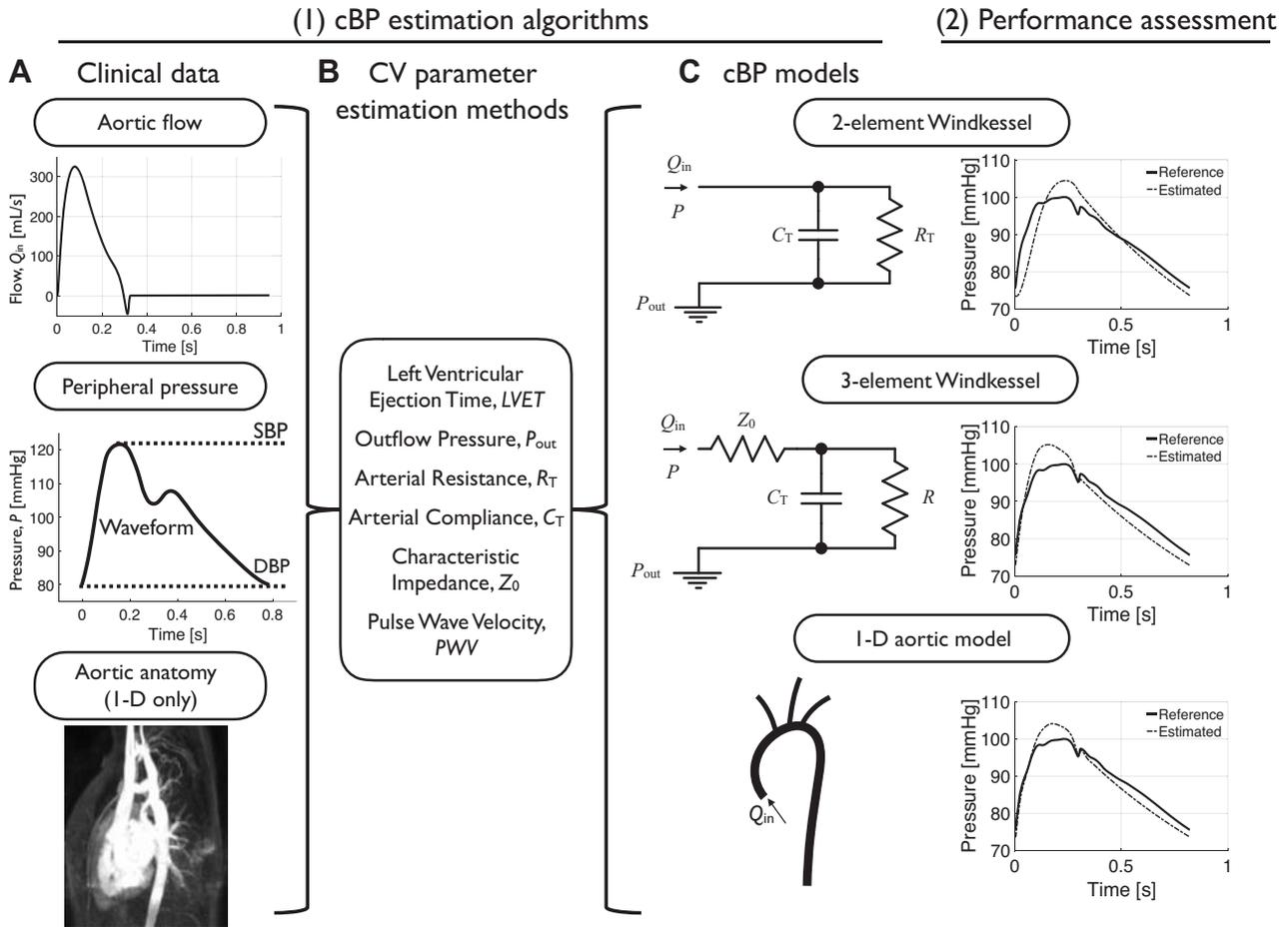
**Figure 1.** Study methodology. *1*) Central blood pressure (cBP) estimation algorithms consisted of three steps. *A*: clinical data acquisition and preprocessing: blood flow measured at the ascending and descending [one-dimensional (1-D) algorithm only] aorta; peripheral blood pressure (BP) measurement; and aortic anatomy (1-D algorithm only). *B*: cardiovascular (CV) parameters estimated from clinical data. *C*: these parameters, along with the noninvasive clinical data, were used as inputs to one of three cBP models. *2*) Algorithm performance was assessed by comparing cBP estimates provided by each model to reference values.

were known precisely, was used to initially test existing CV parameter estimation methods and develop new ones. An existing 1-D dataset was used to further test and refine these methods and the cBP estimation algorithms, as it is based on a more physiological model of the arterial circulation (20).

The 0-D dataset was created using a three-element Windkessel model (see, *Central Blood Pressure Estimation Algorithms*). Each virtual subject's cBP wave was simulated using an aortic flow wave generated by the *AorticFlowWave* script (21) based on prescribed values of heart rate (HR) and

**Table 1.** *Datasets' characteristics*

| | Dataset | | | | |
|---|---|---|---|---|---|
| | **Ao Co** | **Normotensive** | **Hypertensive** | **0-D Dataset** | **1-D Dataset** |
| Subjects (males) | 10 (9) | 13 (10) | 158 (80) | 15,582 (N/A) | 4,064 (N/A) |
| Age, yr | 20.8 ± 9.1 | 48.4 ± 9.4 | 46.2 ± 16.7 | N/A | 50 ± 17.1† |
| DBP, mmHg | 53.2 ± 8.9 | 68.4 ± 10.4$^a$ | 81.8 ± 12.8$^a$ | 64.6 ± 9.0 | 75.3 ± 7.3 |
| MBP, mmHg | 69.3 ± 9.7 | 85.6 ± 12.1$^b$ | 102.0 ± 15.8$^b$ | 83.9 ± 11.2 | 94.2 ± 6.7 |
| pSBP, mmHg | 82.0 ± 15.2 | 111.4 ± 17.3$^c$ | 129.6 ± 22.6$^c$ | 117.6 ± 21.3 | 119.3 ± 11.4 |
| cSBP, mmHg | 93.7 ± 11.9 | 107.2 ± 17.3 | 126.4 ± 22.2 | | 110.4 ± 12.5 |
| pPP, mmHg | 30.6 ± 13.0 | 43.2 ± 12.2 | 48.2 ± 16.0 | 52.9 ± 16.9 | 46.5 ± 14.1 |
| cPP, mmHg | 40.5 ± 12.7 | 38.8 ± 11.0 | 44.6 ± 15.4 | | 35.1 ± 15.3 |
| SV, mL | 57.4 ± 29.9 | 100.6 ± 35.3 | 83.3 ± 32.8 | 88.4 ± 12.2 | 60.3 ± 12.3 |
| HR, beats/min | 65.1 ± 14.4 | 62.2 ± 11.2 | 65.5 ± 10.4 | 68.8 ± 11.3 | 75.9 ± 9.3 |
| CO, L/min | 3.6 ± 1.7 | 6.2 ± 2.5 | 5.3 ± 1.9 | 6.1 ± 1.3 | 4.6 ± 1.1 |

Ao Co, aortic coarctation dataset; CO, cardiac output; cPP, central pulse pressure; cSBP, central systolic blood pressure; DBP, diastolic blood pressure; HR, heart rate; MBP, mean blood pressure; pPP, peripheral pulse pressure; pSBP, peripheral systolic blood pressure; SV, stroke volume. †Age ranges from 25 to 75 yr, with 10-yr intervals. $^a$Brachial oscillometric measurement. $^b$Radial tonometry measurement. $^c$Carotid tonometry measurement.
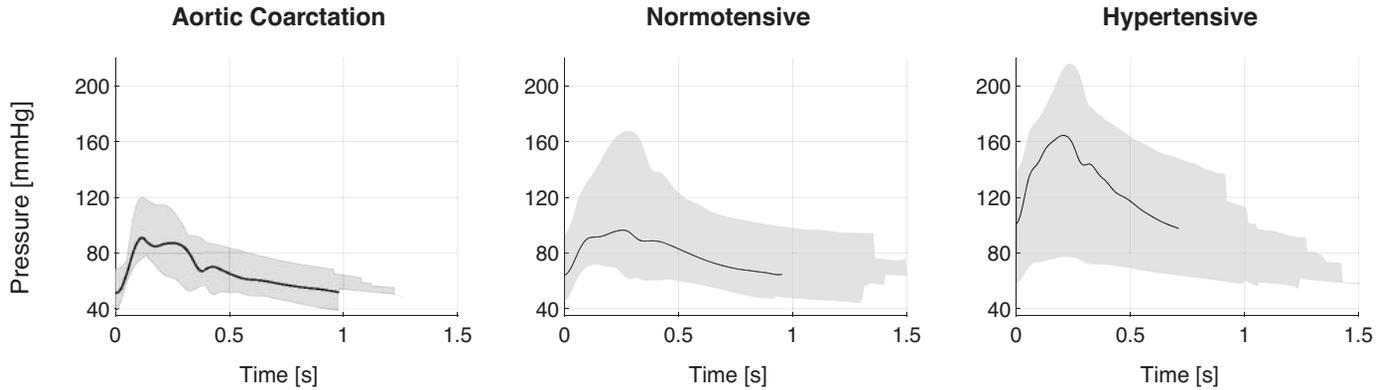
**Figure 2.** Clinical central blood pressure (cBP) wave morphologies: (*left*) aortic coarctation dataset (obtained invasively), (*middle*) normotensive (noninvasive) dataset, and (*right*) hypertensive (noninvasive) dataset. Black lines illustrate a random patient's cBP waveform. Shaded regions represent the range of cBP waves within each dataset.

stroke volume (SV) in combination with prescribed values of $R_T$, $C_T$, $Z_0$, and $P_{out}$. CV parameters were selected to create a dataset of cBP waves representative of a sample of healthy adults. To do so, *1*) mean ($\mu$) and standard deviation ($\sigma$) values of each parameter in healthy adults were identified from the literature (see appendix A); *2*) five values for each parameter were calculated as $\mu$, $\mu \pm 0.5\sigma$, and $\mu \pm \sigma$; and *3*) a virtual subject was created using each of the 15,625 combinations of CV parameters.

The 1-D dataset was created by using a 1-D blood flow model in the aorta and larger arteries of the head and limbs. The CV properties of 25–75-yr-olds were identified through a comprehensive literature review. Pressure, flow velocity, and luminal area waves were simulated in the aorta and other common measurement sites of 4,374 virtual subjects and were verified by comparison against clinical data [see (20) for full details].

We removed nonphysiological data from further analysis, based on limits derived from the hypertensive and normotensive datasets (see Table 1). Maximum limits of central systolic BP (cSBP) and central pulse pressure (cPP) were obtained from the hypertensive dataset. Minimum limits of central diastolic BP (cDBP) and cPP were obtained from the normotensive dataset. Consequently, we excluded subjects with cSBP > 220 mmHg, cDBP < 44 mmHg, and cPP < 18 mmHg
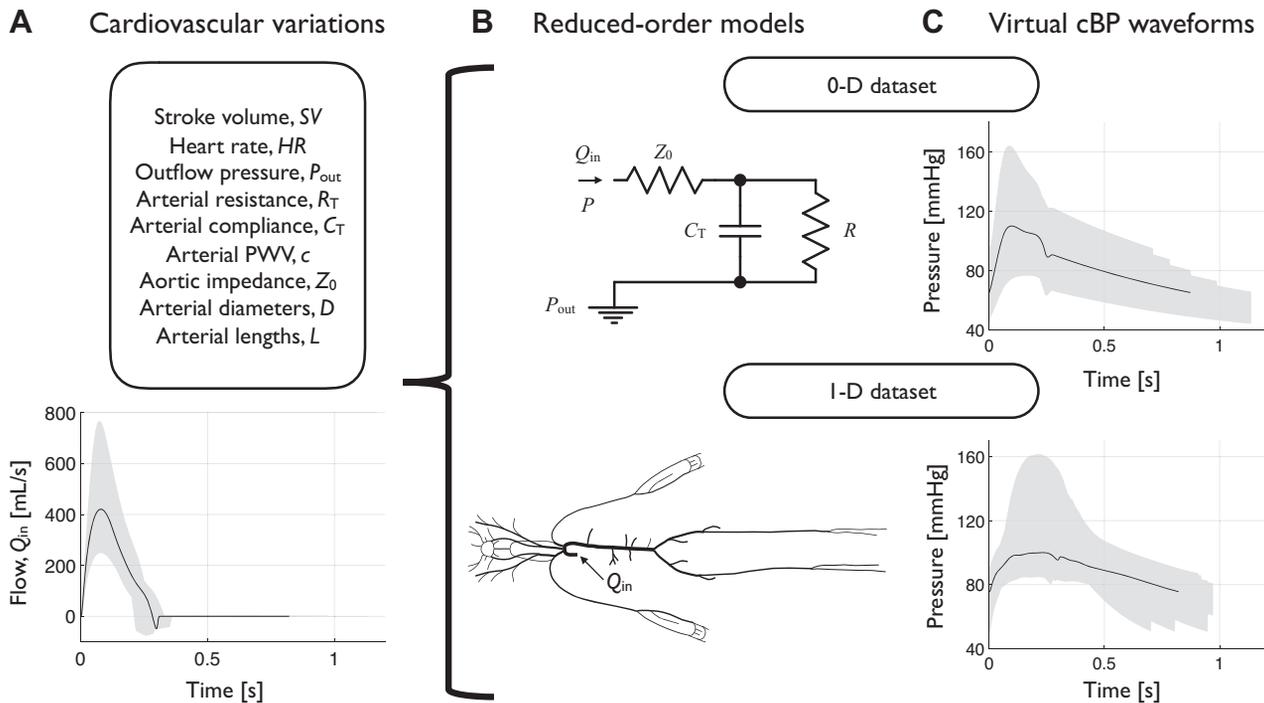


**Figure 3.** Generating datasets of virtual subjects. *A, top*: A range of values for each cardiovascular (CV) parameter was obtained from the clinical literature (see Table A1). *A, bottom*: the thick line illustrates the flow wave corresponding to the baseline values of stroke volume (SV) and heart rate (HR), and the shaded region represents the range of flow waves corresponding to all SV and HR variations. *B*: two reduced-order models were used to generate central blood pressure (cBP) waves. *C*: cBP waves generated by each model: black lines illustrate the cBP wave corresponding to the baseline set of parameter variations, and shaded regions represent the range of cBP waves within each dataset.

or >109 mmHg. Forty-three subjects were excluded from the 0-D dataset; 310 subjects were excluded from the 1-D dataset.

## Cardiovascular Parameter Estimation Methods

The following CV parameters were required as inputs to at least one of the cBP estimation algorithms: LVET, $P_{out}$, $R_T$, $C_T$, $Z_0$, and aortic pulse wave velocity (PWV). A comprehensive literature review of CV parameter estimation methods was performed. The methods listed in Table 2 and described in appendix B were implemented and assessed in this study. To be included, they had to satisfy at least one of the following inclusion criteria: they were reported as the optimal method (22–26), their performance was similar to that of the optimal method (23, 24, 26–28), they were the only reported method (15, 29–47), or their performance had not been sufficiently assessed due to their novelty (32, 35, 37). In addition, new, improved methods were developed.

## Assessing Cardiovascular Parameter Estimation Methods

The performance of the CV parameter estimation methods was assessed using the mean percentage error (MPE) and σ between estimated and reference CV parameter values for the two datasets of virtual subjects. In addition, Bland–Altman plots (48) were created to show the bias and limits of agreement (±1.96 standard deviation from the bias) between estimated and reference CV parameter values. For the 0-D dataset, reference values were obtained from the prescribed values used for each virtual subject (Table A1) (49–52). For the 1-D dataset, reference values for LVET, $P_{out}$, and aortic root PWV were obtained from the prescribed values. $R_T$ was calculated from the aortic root BP and flow waves using (15)

$$R_T = \frac{\text{MBP} - P_{out}}{\overline{Q_{in}}}, \qquad (1)$$

where MBP is the mean blood pressure and $\overline{Q_{in}}$ is the mean blood flow. $C_T$ and $Z_0$ were extracted from aortic root BP and flow waves using the optimized three-element Windkessel model described in appendix A.2.

Two common clinical scenarios were considered when assessing CV parameter estimation methods for each dataset: carotid +, where the carotid BP wave was available, and carotid−, where only brachial DBP and SBP values were available (Fig. 1A). The 1-D dataset of virtual subjects was used to determine, for each scenario and CV parameter, the

**Table 2.** *CV parameter estimation methods assessed in this study*

| Parameter | Description | Sce | Ref | Abb | Percentage Error, % 0-D dataset | Percentage Error, % 1-D dataset |
|---|---|---|---|---|---|---|
| Left ventricular ejection time, LVET | d$P$/d$t$ analysis, 1 | + | (32) | LV1 | ‡ | 0.4 ± 1.0 |
| | d$P$/d$t$ analysis, 2 | + | (37) | LV2 | −12.4 ± 0.1 | −5.7 ± 4.1 |
| | $0.37\sqrt{T}$ | +, − | (31) | LV3 | 26.1 ± 8.5 | 6.9 ± 8.1 |
| | $Q$ analysis | +, − | † | LV4 | 0.1 ± 0.2 | 0.3 ± 0.6 |
| Outflow pressure, $P_{out}$ | Diastolic decay fit, 1 | + | (15, 26) | OP1 | 0.0 ± 0.0 | −5.1 ± 8.0 |
| | Diastolic decay fit, 2 | + | (15, 44) | OP2 | 0.0 ± 0.0 | −10.5 ± 7.5 |
| | 0.5 DBP | +, − | † | OP3 | 1.6 ± 16.9 | 9.1 ± 11.0 |
| | 0.7 DBP | +, − | (56) | OP4 | 42.3 ± 23.6 | 52.7 ± 15.4 |
| Arterial resistance, $R_T$ | (MBP − $P_{out}$)/$\bar{Q}$ | + | (15) | AR1 | 0.0 ± 0.0 | 0.0 ± 0.1 |
| | (DBP + 0.4PP − $P_{out}$)/$\bar{Q}$ | +, − | (22, 15) | AR2 | 0.7 ± 5.7 | −4.9 ± 2.9 |
| Arterial compliance, $C_T$ | 2-point diastolic decay | + | (15) | AC1 | −0.1 ± 0.0 | −6.5 ± 4.9 |
| | Diastolic decay fit, 1 | + | (15) | AC2 | 0.0 ± 0.0 | −6.6 ± 3.3 |
| | Diastolic decay fit, 2 | + | (15, 44) | AC3 | 0.0 ± 0.0 | −10.2 ± 5.0 |
| | Area method | + | (27, 41, 26) | AC4 | −10.0 ± 4.1 | −11.4 ± 4.6 |
| | Two-area method | + | (43, 26) | AC5 | −10.0 ± 4.1 | −7.1 ± 7.1 |
| | DBP method | +, − | † | AC6 | −1.5 ± 4.1 | −17.3 ± 7.5 |
| | PP method | +, − | (25, 26) | AC7 | −0.1 ± 0.2 | −27.6 ± 11.6 |
| | SV/PP | +, − | (27) | AC8 | −13.8 ± 20.3 | 4.9 ± 18.4 |
| | Optimized 3-Wk | + | † | AC9 | 0.0 ± 0.3 | −0.8 ± 4.2 |
| Pulse wave velocity, PWV | Foot-to-foot: $Q_{Ao}$ | +, − | (35) | PV1 | – | 8.2 ± 6.0 |
| | Foot-to-foot: $P_{c-f}$ | +[a] | (35) | PV2 | – | 27.8 ± 10.8 |
| | Least-squares: $Q_{Ao}$ | +, − | (35) | PV3 | – | −12.7 ± 8.3 |
| | Least-squares: $P_{c-f}$ | +[a] | (35) | PV4 | – | 43.0 ± 36.0 |
| | Sum of squares | + | (34) | PV5 | – | 33.2 ± 17.2 |
| Characteristic impedance, $Z_0$ | Frequency methods | + | (29, 33, 23, 36, 38, 40, 24, 42) | Z1 | 2.5 ± 2.1 | 64.6 ± 44.3 |
| | PQ-loop methods | + | (23, 28, 45) | Z2 | 0.2 ± 1.4 | 13.4 ± 56.6 |
| | 0.05 $R_T$ | +, − | (39, 46) | Z3 | −1.5 ± 40.8 | 133.8 ± 66.7 |
| | (MBP − DBP)/$Q_{max}$ | +, − | † | Z4 | −38.7 ± 12.4 | 82.3 ± 32.6 |
| | ρPWV/A | +, − | (47) | Z5 | – | 90.4 ± 18.1 |
| | Optimized 3-Wk | + | † | Z6 | −0.1 ± 0.7 | 37.1 ± 20.0 |

Errors are presented as the means ± SD of the percentage error between estimated and reference CV parameter values. *A*, aortic root cross-sectional area; Abb, coded abbreviations used to refer to each method; DBP, diastolic blood pressure; MBP, mean blood pressure; *P*, peripheral BP waveform; PP, pulse BP values from *P*; $P_{c-f}$, carotid-femoral blood BP wave pair; *Q*, aortic root flow waveform; $\bar{Q}$, mean value of *Q* over *T*; $Q_{Ao}$, ascending and descending aorta flow wave pair; $Q_{max}$, peak aortic flow; Ref, references; Sce, clinical scenarios (+: carotid +, −: carotid−); SV, stroke volume; *T*, duration of cardiac cycle; 3-Wk, 3-element Windkessel; ρ, blood density. Performance was assessed in two clinical scenarios (carotid +: carotid BP wave available; carotid−: only brachial DBP and SBP available) using the 0-D and 1-D datasets (Fig. 1A). †Newly proposed methods (described in appendix B). ‡BP waves from the 0-D dataset do not present a second systolic peak as required by LV1. [a]BP waves at the carotid and femoral arteries required.

optimal (i.e., smallest MPE and $\sigma$) CV parameter estimation methods to be used by the cBP algorithms described in *Central Blood Pressure Estimation Algorithms*.

## Central Blood Pressure Estimation Algorithms

The three algorithms used to estimate cBP each consisted of two stages. First, CV parameters were estimated using the optimal CV parameter estimation methods. Second, a cBP wave was simulated using a computational model of arterial blood flow. We considered the following models: the two-element (15) and three-element (16) Windkessel models and a 1-D model of the thoracic aorta (11), referred to as 1D-Ao hereafter.

### *Two-element Windkessel (0-D) model.*

This model, referred to as 2-Wk hereafter, idealizes the arterial system as a reservoir of compliance $C_T$. Blood flows into the reservoir from the heart, $Q_{in}(t)$, at a pressure $P(t)$, encounters a resistance to flow, $R_T$, and flows out into the vascular beds at a pressure $P_{out}$ (Fig. 1C, *top*). The governing equation is

$$\frac{dP}{dt} + \frac{P - P_{out}}{R_T C_T} = \frac{Q_{in}}{C_T}, \tag{2}$$

which can be solved for $P(t)$ using the integrating factor method,

$$P(t) = P_{out} + (P_0 - P_{out})e^{-\frac{t-t_0}{R_T C_T}} + \frac{e^{-\frac{t}{R_T C_T}}}{C_T}\int_{t_0}^t Q_{in}(t')e^{\frac{t'}{R_T C_T}}dt',$$

$$t \geq t_0, \tag{3}$$

where $t_0$ is the initial time and $P_0 = P(t_0)$.

### *Three-element Windkessel (0-D) model.*

This model, referred to as 3-Wk hereafter, results from adding an impedance, $Z_0$, in series to the 2-Wk model where $R_T = Z_0 + R$ (Fig. 1C, *middle*). $Z_0$ is commonly known as the characteristic impedance and was initially introduced to represent the impedance of the aorta (26). The governing equation is

$$\frac{dP}{dt} + \frac{P - P_{out}}{RC_T} = Z_0\frac{dQ_{in}}{dt} + \frac{(Z_0 + R)Q_{in}}{RC_T}, \tag{4}$$

which can be solved analytically for $P(t)$ using the integrating factor method,

$$P(t) = P_{out} + (P_0 - P_{out} - Z_0 Q_0)e^{-\frac{t-t_0}{RC_T}} + Z_0 Q_{in}(t)$$

$$+ \frac{e^{-\frac{t}{RC_T}}}{C_T}\int_{t_0}^t Q_{in}(t')e^{\frac{t'}{RC_T}}dt', \quad t \geq t_0, \tag{5}$$

where $Q_0 = Q_{in}(t_0)$.

### *1-D aortic model.*

This model uses the 1-D equations of blood flow in the network of compliant vessels shown in Fig. 1C (*bottom*) to compute cBP (11). The inputs to the model are *1*) the geometry (i.e., lengths and cross-sectional areas) of the thoracic aorta, including the supra-aortic arteries; *2*) flow waves at the ascending and descending aortas and, when available, each supra-aortic artery; and *3*) a peripheral BP measurement.

The 1-D and aortic coarctation datasets contained the vascular geometry and PWV data required to run the 1D-Ao algorithm. For the aortic coarctation dataset, the geometry of the thoracic aorta was extracted from MRI data using an in-house segmentation software (53, 54). Besides, since peripheral BP measurements were not available, the BP acquired invasively in the descending aorta was used instead. For the 1-D dataset, the geometry was extracted from the corresponding arterial segments. For both datasets, volumetric blood flow waves were obtained at the ascending ($Q_{in}$, acquired as close to the aortic root as possible) and descending thoracic ($Q_{out}$) aortas. $Q_{in}$ and $Q_{out}$ were used to calculate the pulse wave velocity, PWV, as described in Table 2.

$Q_{in}$ was imposed as an inflow boundary condition at the aortic root and 3-Wk models were coupled to the outlet of each terminal 1-D model segment. The parameters of each outflow model $j$, $Z_{0,Wk}^j$, $C_{T,Wk}^j$ and $R_{Wk}^j$, were calculated using $Q_{in}$, $Q_{out}$, and the outflow distribution (OD) in the supra-aortic arteries, $OD_{flow}^j = \bar{Q}_{out}^j/\bar{Q}_{in}$, under the assumption that DBP, MBP, and $P_{out}$ remain constant within large arteries (1). We used the following equations (11):

$$Z_{0,Wk}^j = \frac{\rho PWV}{A_{out}^j}, \tag{6}$$

$$R_{Wk}^j = \frac{R_T}{OD^j} - Z_{0,Wk}^j, \tag{7}$$

$$C_{T,Wk}^j = (C_T - C_{T,art})\frac{R_T}{R_{Wk}^j}, \tag{8}$$

where $C_{T,art}$ is the total compliance of the 1-D model arterial segments calculated as the sum of each segment compliance,

$$C_{T,art}^k = \frac{\bar{A}^k L^k}{\rho PWV^2}, \tag{9}$$

with $\bar{A}^k$ the average area and $L^k$ the length of the arterial segment $k$. When $\bar{Q}_{out}^j$ were unavailable at each outflow $j$, the difference between the mean values of $Q_{in}$ and $Q_{out}$ was distributed among the supra-aortic arteries proportionally to their outlet areas, $A_{out}^j$, as $OD_{area}^j = (\bar{Q}_{in} - \bar{Q}_{out})A_{out}^j/\Sigma^j A_{out}^j$.

## Assessing Central Blood Pressure Estimation Algorithms

The performance of each cBP estimation algorithm was assessed by comparing estimated cBP values with corresponding reference values in all clinical datasets and in the 1-D dataset. Performance was quantified using the $\mu$ and the $\sigma$ of the errors for central diastolic (cDBP) and systolic (cSBP) blood pressure. In addition, the root mean square error (RMSE) between estimated and reference cBP waves was computed. Similar to *Assessing Cardiovascular Parameter Estimation Methods*, Bland–Altman plots were used to show the bias and limits of agreement between estimated and reference BP values. Finally, the correlation between estimated and reference cBP values was assessed using the coefficient of determination ($R^2$).

## RESULTS

### Assessment of CV Parameter Estimation Methods

The last two columns of Table 2 show mean percentage error (MPE) and standard deviation ($\sigma$) for all CV parameter estimation methods assessed in the two datasets of virtual subjects. MPE for the 1-D dataset was reduced by at least 40% if the carotid BP wave (carotid + ) was used instead of brachial DBP and SBP values (carotid−).

Table 3 displays the methods that led to the smallest MPE for each clinical scenario and dataset. By using these optimal methods, all six CV parameters were calculated in less than 1s for each virtual subject and in less than 1 h for the entire 0-D or 1-D dataset using a Dell Precision M4800 laptop (Round Rock, TX).

All parameters from the 0-D dataset were estimated with MPE < 2% in both clinical scenarios (Table 3, *top*). Figure 4 shows Bland–Altman plots for all CV parameters estimated using the optimal methods obtained from the 1-D dataset (Table 3, *bottom*). These methods were then used in the cBP estimation algorithms (see *Assessment of cBP Algorithms*).

For both scenarios, LVET, $P_{out}$, $R_T$, $C_T$, and PWV were estimated without any considerable bias of their corresponding reference mean values (<6% for carotid + and <10% for carotid−). However, $Z_0$ was overestimated with a much greater bias of its corresponding reference mean value (13% for carotid + and 82% for carotid−). The bias as a function of each CV parameter reference value remained approximately unchanged, with the exceptions of $P_{out}$ (which had a singular reference value) and $C_T$ for carotid− (whose absolute bias increased with increasing reference values). The same optimal methods were identified for PWV in both scenarios.

### Assessment of cBP Algorithms

The cBP algorithms used the optimal CV parameter estimation methods obtained from the 1-D dataset (Table 3, *bottom*). Table 4 shows the estimation errors for all three cBP algorithms, with each algorithm evaluated in four datasets for both clinical scenarios. In the 1-D dataset, RMSEs for carotid + ($\mu \pm \sigma$: < 3.4 ± 1.7 mmHg) were lower than those for carotid− (<5.1 ± 2.5 mmHg). In the clinical datasets, RMSEs were similar for both scenarios and larger than those obtained in the 1-D dataset. The 1D-Ao algorithm led to the smallest RMSEs in the 1-D (2.0 ± 1.0 mmHg) and aortic coarctation (6.4 ± 2.8 mmHg) datasets. The 3-Wk algorithm led to the smallest RMSEs in the normotensive (5.9 ± 2.4 mmHg) and hypertensive (5.7 ± 2.4 mmHg) datasets (these did not

contain the aortic geometry data needed to run the 1D-Ao algorithm).

Overall, estimation errors for cDBP and cSBP were smaller in the 1-D dataset compared with the clinical datasets for all cBP algorithms and clinical scenarios. Furthermore, cDBP errors were smaller than cSBP errors for all algorithms, datasets, and scenarios. However, within each dataset and scenario, cDBP and cSBP errors changed considerably depending on the cBP algorithm used. For both clinical scenarios in the aortic coarctation and 1-D datasets, the 1D-Ao algorithm led to cSBP errors that were smaller or similar compared with the 0-D models (<2.2 ± 5.3 mmHg vs. < 4.5 ± 5.9 mmHg for the 1-D dataset; <2.1 ± 9.7 mmHg vs. <17.3 ± 7.9 mmHg for the aortic coarctation dataset). The 0-D algorithms performed similarly in both datasets and led to smaller cDBP errors than the 1D-Ao algorithm in the aortic coarctation dataset. $R^2$ correlation values between reference and estimated cBP calculated using the best-performing (i.e., 1-D aortic) algorithm and scenario in the 1-D dataset were: 0.834 for cDBP and 0.976 for cSBP (all $P < 0.001$). In the aortic coarctation dataset they were: 0.776 for cDBP and 0.903 for cSBP (all $P < 0.001$).

The normotensive and hypertensive datasets contained noninvasive reference cBP waves calculated by the SphygmoCor device using a transfer function. For carotid−, both 0-D models estimated cDBP and cSBP values with errors <6.0 ± 4.7 mmHg, though the 3-Wk algorithm led to smaller RMSEs in both datasets and scenarios. All errors for the 3-Wk algorithm were larger for carotid + . $R^2$ correlation values for these clinical datasets using the best-performing 0-D algorithm (i.e., 3-Wk) and scenarios were 0.949 for cDBP and 0.997 for cSBP (all $P < 0.001$).

An extended version of Table 4, which also contains errors for cMBP and cPP, is provided as Supplemental Table S1 (all Supplementary material is available at https://doi.org/10.5281/zenodo.3968540). Bland–Altman plots of cDBP, cSBP, cMBP, and cPP are also available (see Supplemental Figs. S1–S8). Supplemental Fig. S4 shows increases in the absolute bias for cSBP with increasing reference BP values in the 1-D, normotensive, and hypertensive datasets for carotid−. Remaining estimates were less affected by varying reference BP values.

Supplemental Figs. S9–S16 show individual cBP wave estimations by each cBP algorithm for a set of randomly chosen subjects in the 1-D dataset and for all subjects in the aortic coarctation, normotensive, and hypertensive datasets, in both clinical scenarios. Using a Dell Precision M4800 laptop, the 0-D algorithms took less than 1s per patient to compute the cBP wave, whereas the 1D-Ao algorithm took less than

**Table 3.** *Optimal CV parameter estimation methods for both datasets and clinical scenarios*

| Dataset | Sce | Optimal CV Parameter Estimation Methods (MPE, %) | | | | | |
| --- | --- | --- | --- | --- | --- | --- | --- |
| | | LVET | $P_{out}$ | $R_T$ | $C_T$ | PWV | $Z_0$ |
| 0-D dataset | + | LV4 (0.3) | OP1/2 (0.0) | AR1 (0.0) | AC2/3 (0.0) | N/A | Z6 (−0.1) |
| | − | | OP3 (1.6) | AR2 (0.7) | AC7 (−0.1) | N/A | Z3 (−1.5) |
| 1-D dataset | + | LV4 (0.3) | OP1 (−5.1) | AR1 (0.0) | AC9 (−0.8) | PV1 (8.2) | Z2 (13.4) |
| | − | | OP3 (9.1) | AR2 (−4.9) | AC8 (4.9) | PV1 (8.2) | Z4 (82.3) |

$C_T$, arterial compliance; LVET, left-ventricular ejection time; MPE, mean percentage error for the entire dataset; $P_{out}$, outflow BP; PWV, pulse wave velocity; $R_T$, arterial resistance; Sce, clinical scenarios ( + : carotid + , −: carotid−); $Z_0$, characteristic impedance. The abbreviations for each method (e.g., LV4) correspond to those described in Table 2.
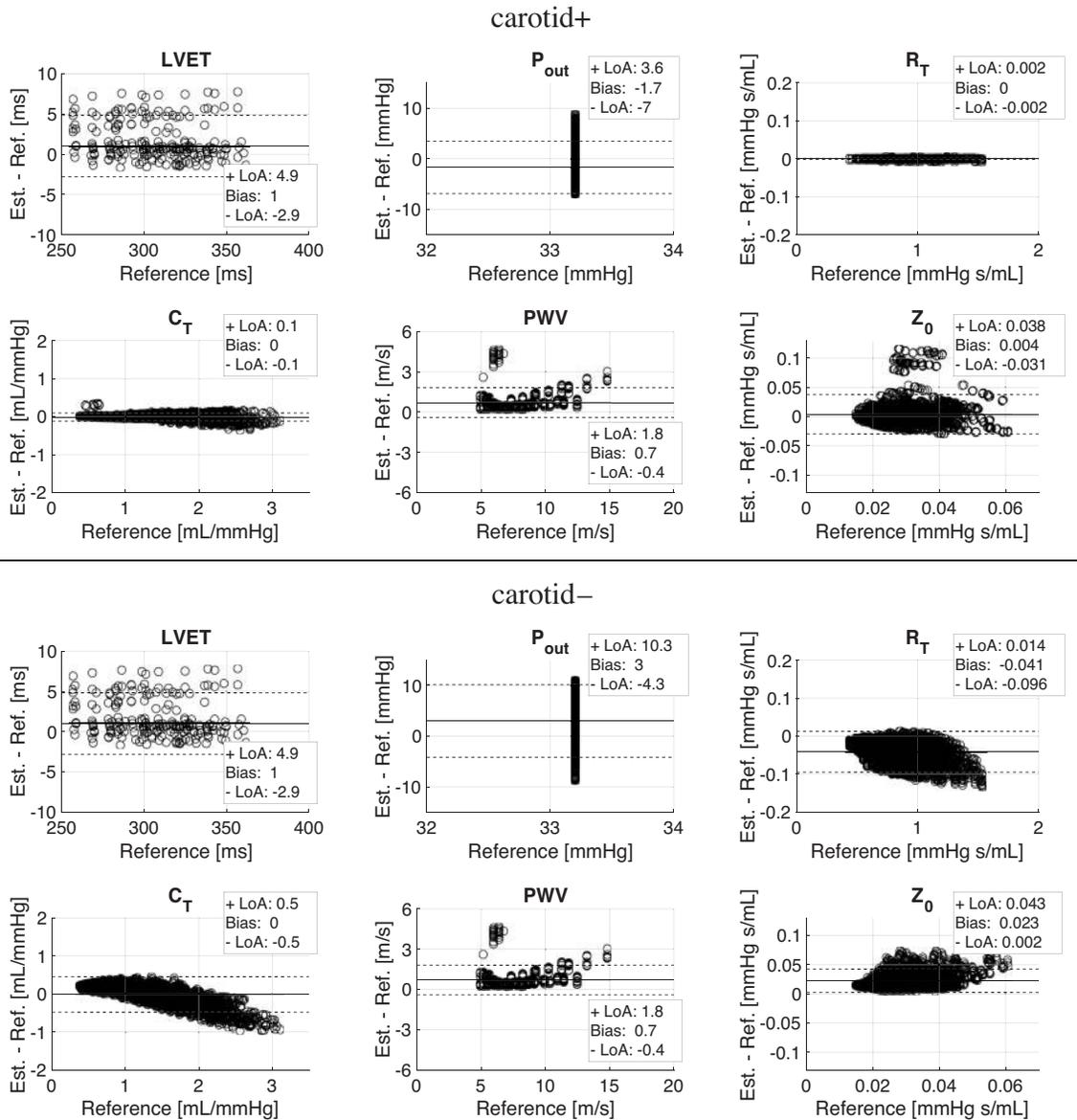
**Figure 4.** Bland–Altman plots for the optimal cardiovascular (CV) parameter estimation methods. They were obtained from all one-dimensional (1-D) dataset waves using the clinical scenarios carotid+ (*top*) and carotid− (*bottom*).

1 min (both times include the time required to calculate all patient-specific CV parameters).

## DISCUSSION

We have developed fast algorithms to estimate several clinically relevant hemodynamic parameters of the systemic circulation and reconstructed the cBP wave from noninvasive data. Our algorithms are based on physical phenomena occurring in the thoracic aorta and are patient specific for all physical parameters except for blood density and viscosity. We have tested them in several in silico and clinical datasets with a wide range of cBP wave morphologies. The 1D-Ao algorithm outperformed the 0-D algorithms at estimating cBP wave morphology when the aortic vascular geometry was available. Both 0-D models estimated cBP values with similar errors when only the aortic flow and peripheral BP

waves were available, though the 3-Wk algorithm produced the smallest RMSEs. The aortic characteristic impedance was the most challenging CV parameter that needed to be estimated, limiting the ability of the 3-Wk algorithm to achieve smaller cBP errors. The novel Windkessel model dataset and optimized cBP algorithms are a valuable resource for developing and testing new, improved algorithms to estimate CV parameters and cBP waves.

### Cardiovascular Parameter Estimation Methods

Obtaining reliable in vivo reference values for the CV parameters required to estimate cBP is challenging. We, therefore, assessed the accuracy of several CV parameter estimation methods using datasets of virtual subjects for which theoretical reference values were either known exactly (all parameters for the 0-D dataset; LVET, $P_{out}$, and PWV for the 1-D dataset) or could be estimated from the

**Table 4.** *Performance of cBP estimation algorithms*

| Dataset | Scenario | Algorithm | Estimation Error ($\mu \pm \sigma$), mmHg | | |
|---|---|---|---|---|---|
| | | | cDBP | cSBP | RMSE |
| 1-D dataset | Carotid + | 2-Wk | $1.2 \pm 0.7$ | $1.0 \pm 0.8$ | $3.4 \pm 1.1$ |
| | | 3-Wk | $0.1 \pm 1.0$ | $1.8 \pm 1.9$ | $2.0 \pm 1.7$ |
| | | 1D-Ao | $0.1 \pm 1.1$ | $2.2 \pm 1.8$ | $2.0 \pm 1.0$ |
| | Carotid − | 2-Wk | $0.8 \pm 1.5$ | $-4.5 \pm 5.9$ | $5.0 \pm 2.5$ |
| | | 3-Wk | $-2.6 \pm 0.8$ | $-0.2 \pm 4.7$ | $5.1 \pm 2.0$ |
| | | 1D-Ao | $-1.5 \pm 1.2$ | $-1.7 \pm 5.3$ | $4.2 \pm 2.1$ |
| Aortic Coarctation | Carotid + | 2-Wk | $0.8 \pm 3.1$ | $-15.7 \pm 7.2$ | $10.1 \pm 3.9$ |
| | | 3-Wk | $0.2 \pm 2.8$ | $-15.4 \pm 7.4$ | $8.0 \pm 3.2$ |
| | | 1D-Ao | $-3.4 \pm 4.8$ | $-0.0 \pm 9.7$ | $6.4 \pm 2.8$ |
| | Carotid − | 2-Wk | $-1.5 \pm 2.4$ | $-17.3 \pm 7.9$ | $10.9 \pm 4.3$ |
| | | 3-Wk | $-1.8 \pm 2.5$ | $-17.2 \pm 7.9$ | $8.4 \pm 3.6$ |
| | | 1D-Ao | $-6.1 \pm 2.8$ | $-2.1 \pm 9.2$ | $7.8 \pm 3.3$ |
| Normotensive | Carotid + | 2-Wk | $4.7 \pm 1.9$ | $-8.6 \pm 5.0$ | $10.3 \pm 3.0$ |
| | | 3-Wk | $-4.4 \pm 3.5$ | $13.4 \pm 13.4$ | $8.6 \pm 5.5$ |
| | Carotid − | 2-Wk | $-0.1 \pm 0.5$ | $-3.3 \pm 3.5$ | $11.0 \pm 3.5$ |
| | | 3-Wk | $0.2 \pm 0.5$ | $-3.7 \pm 4.0$ | $5.9 \pm 2.4$ |
| Hypertensive | Carotid + | 2-Wk | $5.0 \pm 3.2$ | $-8.3 \pm 6.3$ | $10.6 \pm 4.1$ |
| | | 3-Wk | $-2.9 \pm 3.6$ | $8.0 \pm 10.6$ | $7.1 \pm 4.2$ |
| | Carotid − | 2-Wk | $-0.3 \pm 0.8$ | $-5.5 \pm 4.0$ | $11.1 \pm 4.2$ |
| | | 3-Wk | $0.0 \pm 0.6$ | $-6.0 \pm 4.7$ | $5.7 \pm 2.4$ |

Results are presented as mean ($\mu$) and standard deviation ($\sigma$) errors between estimated and reference values of cDBP and cSBP. The RMSE between estimated and reference cBP waves is shown in the last column. Each cBP algorithm was assessed in four datasets and two clinical scenarios: carotid + (peripheral BP wave available) and carotid − (only peripheral SBP and DBP available). cDBP, central diastolic blood pressure; cSBP, central systolic blood pressure; RMSE, root mean square error.

aortic BP and flow waves without measurement error ($R_T$, $C_T$, and $Z_O$ for the 1-D dataset). Unlike the 0-D models, the 1-D model accounts for wave propagation phenomena and can capture high-frequency features of the pressure wave such as the first systolic shoulder, thus providing information that can be derived through pulse wave analysis. The 1-D dataset, therefore, provided the optimal combination of methods for the cBP algorithms and identified accurate methods for estimating CV parameters that, by themselves, can be used to assess cardiovascular function from noninvasive data available in the clinic.

Left ventricular ejection time (LVET) is a valuable metric of left ventricular performance both in health and disease (55). According to our results, it can be estimated accurately from the aortic flow wave using the novel LV 4 method (MPE $\pm \sigma$: $0.3 \pm 0.6\%$).

The physiological meaning and range of values of the asymptotic BP ($P_{out}$) are still not fully understood (56). According to some studies, $P_{out}$ is related to capillary and venous BP (57), though others argue this pressure is larger than the venous BP due to waterfall effects (58–60). We have found that estimation methods based on an exponential fit to the diastolic part of the BP wave outperformed those using a percentage of DBP ($-5.1 \pm 8.0\%$ vs. $9.1 \pm 11.0\%$).

Arterial resistance ($R_T$) is also an important parameter for assessing small blood vessel function (61, 62). According to our results, calculation of $R_T$ from peripheral DBP and SBP values underestimated reference $R_T$ values by 5% on average. More accurate estimates could be obtained when using the whole peripheral BP wave ($0.0 \pm 0.1\%$).

Changes in arterial compliance ($C_T$) can have important effects on the pulse wave, left ventricular dynamics, cardiac output, and the ratio of systolic to diastolic flow into capillary beds (63). Our proposed optimized 3-Wk method for estimating $C_T$ led to a MPE = $-0.8 \pm 4.2\%$, outperforming existing methods. Similar to the study by Stergiopulos et al. (64), we found MPE < 12% for the diastolic decay, area, and two-area methods, though our MPE for the pulse pressure method was higher (27% vs. 17%).

Pulse wave velocity (PWV) provides a direct measure of aortic stiffness and is an independent predictor of cardiovascular risk (65, 66). We found that methods for estimating PWV that used the ascending and descending aorta flows outperformed those using the carotid and femoral BP waves, in agreement with the study by Obeid et al. (67), which also involved in silico data and theoretical reference PWV values.

Aortic characteristic impedance ($Z_O$) is directly related to aortic stiffness (40, 68). In the 1-D dataset, the PQ-loop methods led to smaller MPE (13.4%) than other methods (>37.1%), including those with MPE < 3% when run on the 0-D dataset. Most methods involving BP and flow waves require these to be measured simultaneously at the same location, but in this study, BP was taken from the periphery and combined with the aortic flow wave, resulting in large MPE for the 1-D dataset (>13.4%). PQ-loop methods only require a linear proportionality between aortic BP and flow in early systole, which, according to our results, is maintained between peripheral BP and aortic flow. In fact, BP and flow morphology in early systole are mainly dictated by the propagation of a pulse wave traveling from the heart to the periphery, with the backward-traveling wave having little influence (69). This observation led to the derivation of the novel method Z4, which provided the smallest MPE for carotid− ($82.3 \pm 32.6\%$).

Finally, we note that all CV parameters were estimated individually from the clinical data. However, due to the interdependence between some CV parameters (e.g., $R_T$ and

$P_{out}$), performance may be improved via simultaneous or iterative estimation, as suggested by Parragh et al. (56), though this was beyond the scope of our study.

## Central Blood Pressure Algorithms

We have developed algorithms that estimate the cBP wave from noninvasive, patient-specific measurements by using 0-D and 1-D blood flow modeling. 0-D models were chosen for their simplicity and low number of CV parameters that have to be estimated. The 1D-Ao model was chosen because it captures pulse wave propagation phenomena, though at the expense of a much larger number of parameter estimations. Only the thoracic aorta was simulated using 1-D model segments since cardiac MRI usually provides vessel anatomy and blood flow in the upper part of the aorta only. Furthermore, previous work has shown that it is possible to reduce the topological complexity of the arterial network and, hence, the number of parameters to be estimated, while sufficiently capturing relevant BP values such as cSBP and cPP (70, 71).

We tested the cBP algorithms in several clinical datasets to cover a wide range of cBP wave morphologies, including those seen in hypertensive subjects and in normotensive subjects under the effect of four inotropic and vasoactive drugs that significantly affect BP wave morphology (72). When the aortic vascular geometry was available, the 1D-Ao algorithm outperformed the 0-D algorithms at estimating cBP wave morphology as well as cSBP values, leading to RMSEs $< 2.0 \pm 1.0$ mmHg in the 1-D dataset and $< 6.4 \pm 2.8$ mmHg in the aortic coarctation dataset. When the aortic vascular geometry was unavailable, the three-element 0-D algorithm achieved RMSEs $< 2.0 \pm 1.7$ mmHg for in silico data and $< 5.9 \pm 2.4$ mmHg for clinical data from the normotensive and hypertensive datasets.

Relative errors for cBP estimates were smaller in the 1-D dataset than in the clinical datasets since all hemodynamic data in the former were free of measurement error and inconsistencies that are inherent to clinical datasets (e.g., heart rate differences between pressure and flow waves) (11). Therefore, results obtained from the 1-D dataset provided a theoretical lower bound of cBP errors to be expected when analyzing clinical datasets.

Recent (2017) clinical guidelines for the validation of noninvasive cBP devices propose a mean absolute difference of $\leq 5$ mmHg with $\sigma \leq 8$ mmHg compared with the reference cSBP (19). The potential of the algorithms used in this study to achieve mean absolute differences that are almost within recommended values in clinical cohorts with either invasive reference cBP values (aortic coarctation dataset) or cBP values calculated by the widely used SphygmoCor device (normotensive and hypertensive datasets) has been shown. On the one hand, the 1D-Ao algorithm achieved mean absolute differences $< 2.1 \pm 9.7$ mmHg for cSBP values in the aortic coarctation dataset for both scenarios. On the other hand, the 0-D models achieved mean absolute differences $< 8.6 \pm 5.0$ mmHg in the normotensive dataset and $< 8.0 \pm 10.6$ mmHg in the hypertensive dataset. Furthermore, the lower-bound RMSEs obtained when testing all algorithms in the measurement error-free 1-D dataset were even smaller ($< 3.4 \pm 1.7$ mmHg for carotid $+$ and $< 5.1 \pm 2.5$ mmHg for carotid$-$), suggesting that our algorithms' performance could be within recommended values if measurement error and data inconsistencies could be reduced further during data acquisition.

Central BP estimates for some subjects in the normotensive and hypertensive datasets showed large errors ($> 50$ mmHg). These subjects had noisy ultrasound velocity time integral (VTI) waves (used to calculate aortic flow waves) characterized by either an extended diastolic phase (resulting in LVET $> 50\%$ of the cardiac cycle duration) or a large second peak after the systolic peak. Both artifacts could explain the smaller cBP estimation errors for the 0-D models in the more challenging carotid$-$ scenario compared with carotid $+$.

A review of methods to estimate cSBP from arterial pulse waves (73) found a mean error (95% confidence interval) of $-1.1$ ($-2.8$ to $0.7$) mmHg when calibrated using invasive BP values and a mean error of $-5.8$ ($-7.8$ to $3.8$) mmHg when calibrated using noninvasive BP values. In our study, the 1D-Ao algorithm was found to have mean errors of $0.0$ ($-6.0$ to $6.0$) mmHg when calibrated using an invasive BP waveform (carotid $+$ scenario in the aortic coarctation dataset) $-2.1$ ($-7.8$ to $3.6$) mmHg when using invasive BP values (carotid$-$ scenario in the aortic coarctation dataset), and the 2-Wk algorithm was found to have mean errors when calibrated noninvasively of $-3.3$ ($-3.9$ to $-2.7$) mmHg (carotid$-$ scenario in the normotensive dataset) and $-5.5$ ($-6.1$ to $-4.9$) mmHg (carotid$-$ scenario in the hypertensive dataset). Thus, the mean cSBP error provided by the models presented in this study was comparable with those observed in previous studies of cSBP estimation methods. Unlike transfer function methods, our proposed cBP algorithms do not need to be trained on existing clinical datasets and make no assumptions regarding generalizability, since they simulate patient-specific hemodynamic phenomena occurring in the aorta where cBP is calculated. This may be advantageous when applying these algorithms to the wider population, including patients suffering from a range of CV diseases or under pharmacological treatment. However, a direct comparison against such techniques was not possible due to the lack of required data and corresponding devices.

## Limitations

The peripheral pressure wave ($P$) required by the cBP algorithms was measured invasively in the descending aorta in the aortic coarctation dataset. Since this may give the algorithms an advantage compared with noninvasive methods using cuff or tonometry measurements, the 1-D dataset—which contained $P$ at the required peripheral locations—was also used for the final cBP algorithm assessment. In the normotensive and hypertensive datasets, since invasive reference cBP measurements were not available, noninvasive measurements were obtained using the SphygmoCor device. Although these measurements are not exactly equivalent to invasive cBP, they allowed us to compare the performance of the cBP algorithms to a widely used noninvasive device. We note that the aortic coarctation dataset contained data from 10 subjects—in the future, further studies should verify the conclusions presented here using additional data with invasive reference measurements.

## Perspectives

Patients with cardiovascular disease would benefit from an accurate noninvasive assessment of their cBP. Our approach removes the risk of complications due to cardiac catheterization and allows for a more regular assessment of a patient's cBP, due to its noninvasive nature. Moreover, it is relatively quick: it only takes a few seconds (when using the 0-D algorithms) or a few minutes (when using 1D-Ao algorithm) to compute cBP on a Dell Precision M4800 laptop. The 1-D algorithm is particularly relevant in clinical cardiology, where cardiac MRI is increasingly used. Indeed, the detailed geometric and flow data obtained using MRI can lead to important improvements in noninvasive cBP estimation, which could lead to a better adaption in clinical practice. In addition, the 0-D algorithms can be used in combination with US scans to obtain patient-specific cBP estimates.

The novel Windkessel model dataset and optimized cBP algorithms are freely available (see DATA ACCESS STATEMENT) to develop and test new, improved algorithms for estimating CV parameters and cBP waves.

## Conclusion

We have presented freely available, fast, patient-specific algorithms to estimate clinically relevant CV parameters and reconstruct the cBP wave from the aortic flow wave, using noninvasive data and patient-specific models of aortic blood flow. We have tested our algorithms against a wide range of cBP morphologies from several clinical datasets, one of which included catheter cBP waves. Finally, we have shown the potential of our algorithms to estimate cBP values within guideline-recommended values. Our approach could improve CV function assessment in clinical cohorts for which aortic ultrasound or magnetic resonance imaging data are available.

## APPENDIX

## APPENDIX A: DATASETS OF VIRTUAL SUBJECTS

### Appendix A.1. 0-D Dataset: CV Parameter Variations

## Appendix A.2. 1-D Dataset: Calculating Reference $Z_O$ and $C_T$ Values at the Aortic Root

Reference $Z_O$ and $C_T$ values for the 1-D dataset were calculated from aortic root BP ($P$) and flow ($Q_{in}$) waves using an in-house algorithm written in MATLAB and based on the 3-Wk model (Fig. A1). Assuming that $P_{out}$ is known and that the total resistance $R_T = Z_O + R$ is given by Eq. 1, a parameter estimation problem can be solved for $Z_O$ and $C_T$. The estimated BP at time $t_k$ can be written as

$$P(t_k) = f\left(Z'_0, C'_T, Q_{in}(t_k)\right) + e_k, \qquad (A1)$$

with $e_k$ the residual error between the estimated and reference BP at each time $t_k$, $k = 1, \ldots, K$, and $Z_0'$ and $C_T'$ the estimated parameters. The problem can be solved through iterative minimization of the cost function $\mathbf{e}^\top\mathbf{e}$, where $\mathbf{e}$ is the vector containing the residual errors at each time $t_k$. The iterative procedure starts from an initial estimate $\left(Z'_{0,0}, C'_{T,0}\right)$. The parameters at iteration $i + 1$ are then calculated using the recursive equation

$$\left(Z'_{0,i+1}, C'_{T,i+1}\right) = \left(Z'_{0,i}, C'_{T,i}\right) - \mathbf{H}_i\mathbf{q}_i, \qquad (A2)$$

where $\mathbf{H}_i$ and $\mathbf{q}_i$ are the Hessian and the gradient, respectively, of the cost function evaluated at iteration $i$. This equation can be obtained by approaching the cost function by a second-order Taylor expansion and minimizing the approached function. The mean cBP difference shown in Fig. A1, B and C, was calculated for each iteration as $\frac{1}{K}\sqrt{\sum_{k=1}^{K} e_k^2}$, with $e_k$ the residual error at time $t_k$. The iterative procedure was stopped when either 1) the change in both $Z_0$ and $C_T$ estimates between iterations was smaller than $10^{-6}$ or 2) after 15 iterations.

## APPENDIX B: CARDIOVASCULAR PARAMETER ESTIMATION METHODS

All CV parameter estimation methods used in this study are described next. Novel methods are marked with an asterisk in the title.

**Table A1.** *CV parameter variations used for the three-element Windkessel (0-D) dataset*

| CV parameter, units | Negative $\mu - \sigma$ | $\mu - 0.5\sigma$ | Baseline $\mu$ | Positive $\mu + 0.5\sigma$ | $\mu + \sigma$ | References |
|---|---|---|---|---|---|---|
| SV, mL | 71.2 | 79.8 | 88.4 | 97.0 | 105.7 | (52) |
| HR, beats/min | 52.9 | 60.8 | 68.8 | 76.7 | 84.7 | (52) |
| $P_{out}$, mmHg | 31.7 | 32.5 | 33.2 | 34.0 | 34.7 | (51) |
| $R_T$, mmHg·s/mL | 0.468 | 0.484 | 0.500 | 0.516 | 0.532 | (44) |
| $C_T$, mL/mmHg | 2.20 | 2.23 | 2.27 | 2.30 | 2.34 | (50) |
| $Z_O$, mmHg·s/mL | 0.0256 | 0.0358 | 0.0485 | 0.0644 | 0.0847 | (65, 49) |

$\mu$ and $\sigma$ are mean and standard deviation values, respectively, for each CV parameter from the clinical literature. $C_T$: total arterial compliance; HR: heart rate; $P_{out}$: outflow vascular pressure; $R_T$: total arterial resistance; SV: stroke volume; $Z_O$: aortic characteristic impedance. These values are based on observations in healthy humans from the clinical literature.
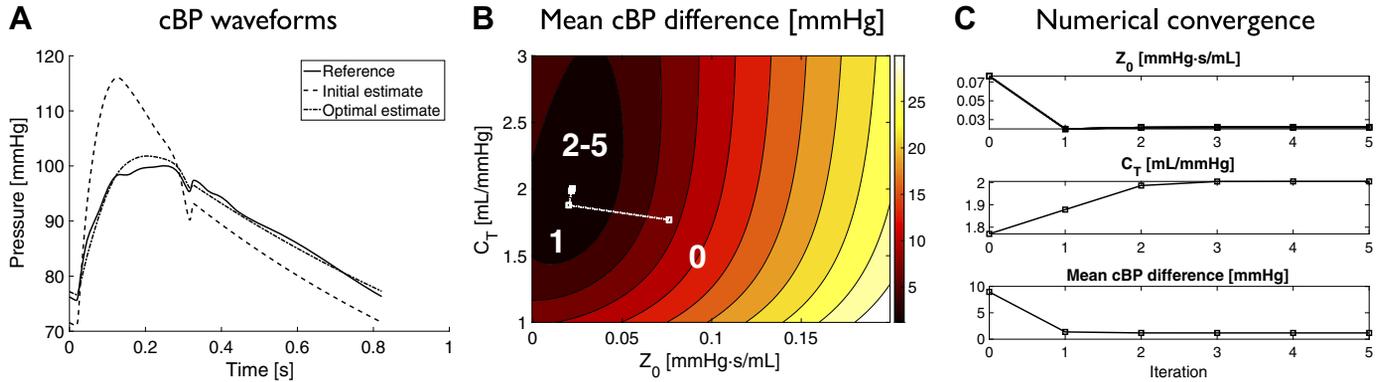
**Figure A1.** Extracting reference aortic characteristic impedance ($Z_0$) and total arterial compliance ($C_T$) values at the aortic root. *A:* reference central blood pressure (cBP) wave for a one-dimensional (1-D) model virtual subject, and corresponding initial and optimal estimates. *B:* contour plot (in mmHg) of the mean difference between the estimated and reference cBP waves, with $Z_0$ in the *x*-axis and $C_T$ in the *y*-axis. Each iteration is shown in white squares; iterations 0 and 5 correspond to the initial and optimal cBP estimates, respectively. *C:* the values of $Z_0$, $C_T$, and the cBP mean difference are shown for the initial estimate and for every iteration until numerical convergence is reached.

## Appendix B.1. LV—Left Ventricular Ejection Time, LVET

### LV1—dP/dt analysis, 1*.

The method is described in the work by Charlton et al. (32). LVET corresponds to the point of peak pressure after the pressure systolic peak.

### LV2—dP/dt analysis, 2.

This method is described in the work by Itu et al. (37). LVET coincides with the minimum of

$$\frac{dP}{dt}\left(0.5 - \left|0.5 - \frac{HR \cdot t}{60}\right|\right)^2, \qquad (B1)$$

where $P$ is a peripheral BP wave and HR represents the heart rate in beats/min.

### LV3—$0.37\sqrt{T}$.

LVET is calculated using the empirical relationship described in the work by Bazett (31): $0.37\sqrt{T}$, where $T$ is the duration of the cardiac cycle in seconds.

### LV4—Q analysis*.

$Q$ is analyzed from the global minimum after peak flow to 50% of $T$ (Fig. B1). If all $Q$ values are smaller than 1% of maximum $Q$, LVET corresponds to the time of the global minimum. Otherwise, starting from the time of the global minimum, all sign changes (from negative to positive), all maxima, and all zero values are found. LVET corresponds to either the first sign change, the first local maximum, or the first zero value (whichever one occurs first). If all else fails, method LV 3 is used.

## Appendix B.2. OP—Outflow Pressure

### OP1—diastolic decay fit, 1.

The concept of a diastolic decay fit was first described by Frank (15). $P$ is analyzed between LVET and the end of diastole ($P_d$). The multidimensional unconstrained nonlinear minimization (Nelder–Mead) MATLAB function *fminsearch.m* is used to find the best fit between $P_d$ and an exponential decay curve of the form: $P_{exp} = P_{out} + (P_{exp}(t_0) - P_{out})e^{-(t-t_0)/\tau}$, where $t_0$ = LVET. To avoid nonphysiological values of $P_{out}$, the following filters are applied: if $\tau < 0$ or $P_{out} < 0$, $P_{out}$ is set to 0; and if $P_{out} \geq$ DBP, $P_{out}$ is set to 0.5DBP.

### OP2—diastolic decay fit, 2.

Similar to OP1, but using $t_0 = \frac{2}{3}$ LVET $+ \frac{1}{3}T$ instead, as described by Simon et al. (44).

### OP3—50% of DBP*.

$P_{out}$ is estimated as 50% of DBP.

### OP4—70% of DBP.

As suggested by Parragh et al. (56), $P_{out}$ is estimated as 70% of DBP.

## Appendix B.3. AR—Arterial Resistance

### AR1—peripheral pressure waveform.

$R_T$ is calculated using Eq. 1 and MBP is calculated as the mean of $P$.

### AR2—peripheral DBP and SBP values.

Similarly to AR1, but using MBP = 0.4SBP + 0.6DBP instead, as described by Bos et al. (22).

## Appendix B.4. AC—Arterial Compliance

### AC1—2-point diastolic decay.

The concept of a diastolic decay fit was first described by Frank (15). Using only the first and last points of the diastolic part of $P$, $C_T$ is calculated as:

$$\frac{T - LVET}{\ln\left(\frac{P(LVET) - P_{out}}{DBP - P_{out}}\right)R_T}. \qquad (B2)$$

### AC2—diastolic decay fit, 1.

Given that $\tau = (R_T - Z_0)C_T$, OP1 can be used to calculate $\tau$, and rearranging:

$$C_T = \frac{\tau}{R_T - Z_0}. \qquad (B3)$$

If $\tau$ is negative, then $P_{out}$ is set to 0 and $\tau$ is recalculated.

### AC3—diastolic decay fit, 2.

Similar to AC2, but using $t_0 = \frac{2}{3}$ LVET $+ \frac{1}{3}T$ instead, as described by Simon et al. (44).

### AC4—area method.

This method is described by Randall et al. (41). $C_T$ is calculated as:

$$\frac{\int_{t_1}^{t_2}(P - P_{out})\mathrm{d}t}{R_T(P(t_1) - P(t_2))}, \qquad (B4)$$

where $t_1$ and $t_2$ are equal to $\frac{2}{3}$ LVET $+ \frac{1}{3}T$ and 90% of $T$, respectively.

### AC5—two-area method.

This method is described by Self et al. (43). $C_T$ is calculated by solving two simultaneous equations of the form:

$$\int_{t_1}^{t_2}Q\mathrm{d}t - \frac{1}{R_T}\int_{t_1}^{t_2}(P - P_{out})\mathrm{d}t = C_T(P(t_1) - P(t_2)), \qquad (B5)$$

from the start of the cycle to LVET and from LVET to $T$.

### AC6—diastolic blood pressure method[*].

$C_T$ is calculated by minimizing the relative error, $DBP_{err} = (DBP_{est} - DBP_{ref})/DBP_{ref}$, between the estimated ($DBP_{est}$) and reference ($DBP_{ref}$) values of DBP, as seen in Fig. B2. For each iteration, $j$, $DBP_{est}$ is calculated as the minimum of the estimated BP, $P_{est}$, using the three-element Windkessel model (Eq. 5). The initial conditions are $C_{T,0} = SV/PP$ and $P_0 = DBP_{ref}$. While $DBP_{err} > 1\%$, $C_{T,j} = C_{T,j-1}/DBP_{err}^2$. $C_T$ corresponds to the final value of $C_{T,j}$.

### AC7—pulse pressure method.

This method is described by Stergiopulos et al. (25). Similar to AC6, but minimizing the relative PP error, $PP_{err}$, instead.

### AC8—stroke volume over pulse pressure.

This method is described by Chemla et al. (27). $C_T$ corresponds to SV/PP.

### AC9—three-element Windkessel optimization[*].

This method is described in appendix A.2. The initial value of $C_T$ is calculated using AC8.

## Appendix B.5. PV—Pulse Wave Velocity

The foot-to-foot (PV 1 and PV 2) and least-squares (PV 3 and PV 4) methods used here are described by Gaddum et al. (35). Both methods require the measurement of two pulse waves at both ends of a given arterial path of length

$L$. The foot-to-foot method focuses on detecting the feet of both pulse waves to calculate the transit time (TT) between them. For each pulse wave, the foot is detected as the intersection between a horizontal projection of the minimum value and a projection of the maximum slope of the systolic upstroke.

The least-squares method calculates the sum of the squared differences between the systolic upstroke of both waves multiple times, by fixing one wave and shifting the other one by one datapoint at a time. The temporal shift that minimizes the squared differences is used to estimate TT. For both methods, PWV is then calculated as PWV = $L$/TT.

### PV1—foot-to-foot: aortic flow.

The inputs are two noninvasive flow waves at the ascending and descending aortas.

### PV2—foot-to-foot: carotid-femoral pressures.

The inputs are two noninvasive BP waves at the carotid and femoral arteries.

### PV3—least-squares: aortic flow.

The inputs are two noninvasive flow waves at the ascending and descending aortas.

### PV4—least-squares: carotid-femoral pressures.

The inputs are two noninvasive BP waves at the carotid and femoral arteries.

### PV5—sum of squares.

This method has been adapted from the original one described by Davies et al. (34). PWV is calculated from the peripheral BP, $P$, and aortic flow, $Q$ waves using

$$PWV = \frac{1}{\rho A}\sqrt{\frac{\sum \mathrm{d}P^2}{\sum \mathrm{d}Q^2}}, \qquad (B6)$$

where $\rho$ is the blood density, $A$ is the cross-sectional area at the aortic root, $\mathrm{d}P$ and $\mathrm{d}Q$ are differences in $P$ and $Q$, respectively, between two adjacent time points, and the sums extend over a cardiac cycle. $P$ and $Q$ do not need to be aligned in time.

## Appendix B.6. Z—Aortic Characteristic Impedance

Method $Z2$ is sensitive to temporal misalignments between $P$ and $Q$, so the following restrictions were applied to account for waves that were not recorded simultaneously and/or at the same site: 1) $P$ is shifted so that its value at the start of the cycle coincides with DBP, and 2) $Q$ is shifted so that its value at the start of the cycle is as close as possible to the intersection between the $x$-axis and the tangent of $Q$ at the time of maximum $\mathrm{d}Q/\mathrm{d}t$ in early systole.

### Z1—frequency methods.

Frequency domain methods to estimate characteristic impedance ($Z_0$) are based on the Fourier analysis of $P$ and $Q$ extracted simultaneously at the ascending aorta. $Z_0$ is
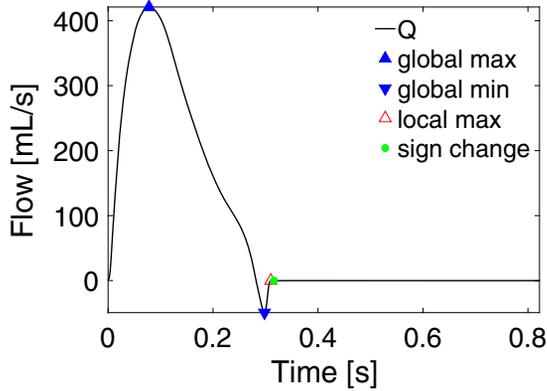
**Figure B1.** Novel method to estimate left ventricular ejection time (LVET) from the aortic flow wave, $Q$. LVET corresponds to the time of the first sign change (green circle), which occurs earlier than the local maximum (red triangle).

usually estimated as the average impedance modulus over a range of frequencies where fluctuations—due to wave reflections—above and below the characteristic impedance value are expected to cancel each other out. The following harmonic ranges, extracted from the literature, have been assessed in this study: 2–12th (40), 6–10th (42), 1–8th (33), 1–9th (23), 2–10th (38), 3–10th (36), 4–10th (45), 6–8th (29), and 4–8th (24) harmonics. These methods, in their original form, require $P$ and $Q$ measured simultaneously at the ascending aorta. However, for the proposed algorithms, a peripheral $P$ measurement is used instead.

### Z2—P-Q loop methods.

*P-Q* loop methods analyze the relationship between aortic $P$ and $Q$ during early systole, assuming that during this interval, the effects of wave reflections are minimal (23, 28), and hence

$$Z_0 \simeq \frac{P(t) - DBP}{Q(t) - Q(0)}, \qquad (B7)$$

where $Q(0)$ is the value of $Q$ at the start of the cycle (normally zero). In this study, four P-Q loop methods were assessed where $Z_0$ was estimated as:

I    the mean value of Eq. *B7* between the start of the cycle and the time of maximum $Q$;
II   the slope of the linear least squares fit to the ratio between $P$ and $Q$ between the start of the cycle and the time of maximum flow;
III  the value of Eq. *B7* at the time of maximum d$Q$/d$t$ in early systole; and
IV   the mean value of Eq. *B7* between the start of the cycle and the time of maximum d$Q$/d$t$ in early systole.

The best-performing *P-Q* loop method, IV, was used to calculate the errors in Table 2. These methods, in their original form, require $P$ and $Q$ measured simultaneously at the ascending aorta. However, for the proposed algorithms, a peripheral $P$ measurement is used instead.

### Z3—5% of $R_T$.

As suggested by Murgo et al. (39), $Z_0$ is estimated as 5% of $R_T$.

### Z4—approximated aortic characteristics*.

During early systole, wave reflections reaching the aortic root are assumed to be absent, and characteristic impedance can be estimated as $Z_0 = \Delta P/\Delta Q$, where $\Delta P$ and $\Delta Q$ are the changes in BP and flow rate, respectively (36). Peak flow, $Q_{peak}$, and the first systolic shoulder/peak, $P1$, occur at a similar time, so $\Delta Q = Q_{peak}$ and $\Delta P = P1$, and therefore, $Z_0 \simeq P1/Q_{peak}$, as seen in Fig. B3. Assuming that DBP and MBP remain constant within the large arteries, $P1$ is approximated as $MBP - DBP$ extracted from a peripheral $P$ measurement. Hence, $Z_0 \simeq (MBP - DBP)/Q_{peak}$.

### Z5—aortic characteristics.

This method is described by Westerhof et al. (47). Assuming that the aortic radius is much larger than the aortic wall thickness, $Z_0$ corresponds to $\rho PWV/A$, where $\rho$ is the blood density, PWV is the aortic pulse wave velocity, and $A$ is the aortic-root cross-sectional area.

### Z6—three-element Windkessel optimization*.

This method is described in appendix A.2. The initial values of $C_T$ and $Z_0$ are calculated using the AC8 and Z3 methods, respectively.

## DATA ACCESS STATEMENT

A data supplement related to this manuscript is publicly available at https://doi.org/10.5281/zenodo.3968540. These materials are not a part of this manuscript and have not undergone peer review by the *American Physiological Society (APS)*. *APS* and the journal editors take no responsibility for these materials, for the website address, or for any links to or from it. The data collected during the literature review and the results from the 0-D and 1-D simulations, together with the MATLAB code used to generate 0-D datasets, to run 0-D simulations, to create input files for 1-D simulations, and to post-process and analyze these data are available here https://github.com/jmariscal-harana/cbp_estimation.
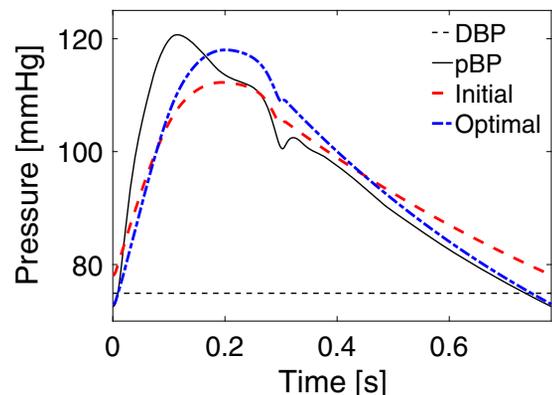


**Figure B2.** Novel iterative method to estimate arterial compliance ($C_T$) from the aortic flow and peripheral blood pressure (pBP) waves. $C_T$ estimates are calculated by minimizing the relative error between the estimated and reference values of diastolic blood pressure (DBP). The latter is obtained from the pBP wave (black dashed line). The BP waves corresponding to the initial and optimal estimates of $C_T$ are shown in red and blue lines, respectively.
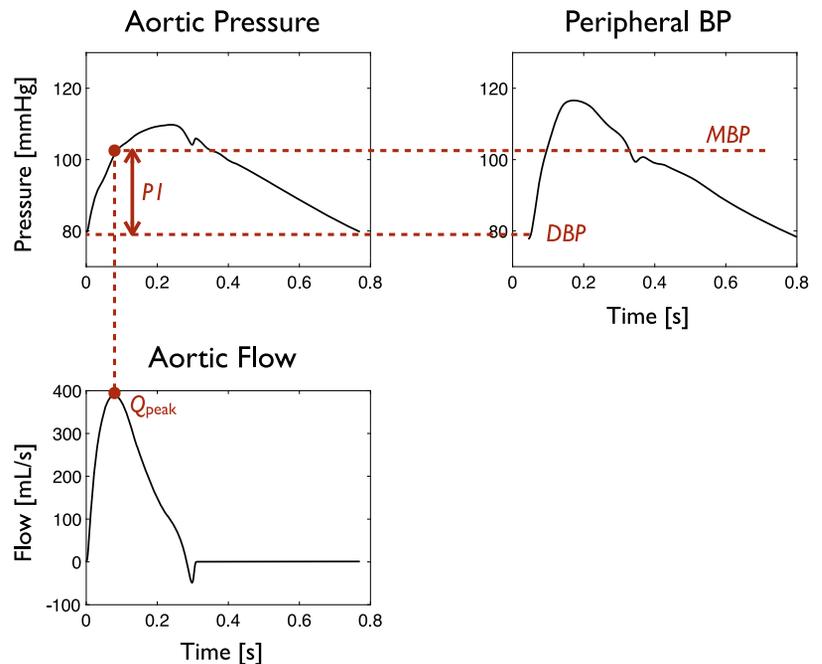
**Figure B3.** Novel method to estimate aortic characteristic impedance from the aortic flow and peripheral blood pressure (BP) waves. Pressure (*top*) and flow (*bottom*) waves at central (*left*) and peripheral (right) arterial locations for a subject from the 1-D dataset. The time of $Q_{peak}$ and $P1$ is indicated by the vertical, red, dashed line. The value of $P1$ is approximated as mean blood pressure (MBP) − diastolic blood pressure (DBP) calculated from the peripheral BP wave.

Details of the code used to run the 1-D simulations are available at http://haemod.uk, and access requests should be addressed to J. Alastruey at jordi.alastruey-arimon@kcl.ac.uk. Details of how to replicate this study can be obtained by contacting J. Mariscal-Harana at jorge.mariscal_harana@kcl.ac.uk. Further information about the data and conditions of access can be found by emailing research.data@kcl.ac.uk.

## DISCLOSURES

No conflicts of interest, financial or otherwise, are declared by the authors.

## AUTHOR CONTRIBUTIONS

J.A. and P.H.C. conceived and designed research; J.M.-H. performed experiments; J.M.-H and A.v.E. analyzed data; J.M.-H, P.H.C., and J.A. interpreted results of experiments; J.M.-H and J.A. prepared figures; J.M.-H, P.H.C., and J.A. drafted manuscript; J.M.-H, J.A., P.H.C., S.V., M.C.F., A.v.E., T.S., B.R., M.C., and J.A. edited and revised manuscript; J.M.-H, P.H.C., S.V., J.A., M.C.F., A.v.E., T.S., H.d.B., B.R., I.V., P.B., H.G., M.C., P.C., S.S., and, J.A approved final version of manuscript.

## REFERENCES

1. **Agabiti Rosei E**, **Fox K**, **Ferrari R.** Understanding and treating central blood pressure. *Dialogues Cardiovasc Med* 20: 169–184, 2015. https://dialogues-cvm.org/wp-content/uploads/2018/04/DCVM77-1.pdf.

2. **McEniery CM**, **Cockcroft JR**, **Roman MJ**, **Franklin SS**, **Wilkinson IB.** Central blood pressure: current evidence and clinical importance. *Eur Heart J* 35: 1719–1725, 2014. doi:10.1093/eurheartj/eht565.

3. **Sharman JE**, **Marwick TH**, **Gilroy D**, **Otahal P**, **Abhayaratna WP**, **Stowasser M; Value of Central Blood Pressure for GUIDing ManagEment of Hypertension Study Investigators.** Randomized trial of guiding hypertension management using central aortic blood pressure compared with best-practice care: principal findings of the BP GUIDE study. *Hypertension* 62: 1138–1145, 2013. doi:10.1161/HYPERTENSIONAHA.113.02001.

4. **Williams B**, **Brunel P**, **Lacy PS**, **Baschiera F**, **Zappe DH**, **Kario K**, **Cockcroft J.** Application of non-invasive central aortic pressure assessment in clinical trials: clinical experience and value. *Artery Res* 17: 1–15, 2016. doi:10.1016/j.artres.2016.10.154.

5. **Herbert A**, **Cruickshank JK**, **Laurent S**, **Boutouyrie P Reference Values for Arterial Measurements Collaboration.** Establishing reference values for central blood pressure and its amplification in a general healthy population and according to cardiovascular risk factors. *Eur Heart J* 35: 3122–3133, 2014. doi:10.1093/eurheartj/ehu293.

6. **Sharman JE**, **Stowasser M**, **Fassett RG**, **Marwick TH**, **Franklin SS.** Central blood pressure measurement may improve risk stratification. *J Hum Hypertens* 22: 838–844, 2008. doi:10.1038/jhh.2008.71.

7. **McEniery CM**, **Yasmin**, **Hall IR**, **Qasem A**, **Wilkinson IB**, **Cockcroft JR ACCT Investigators.** Normal vascular aging: differential effects on wave reflection and aortic pulse wave velocity: the Anglo-Cardiff Collaborative Trial (ACCT). *J Am Coll Cardiol* 46: 1753–1760, 2005. doi:10.1016/j.jacc.2005.07.037.

8. **Itu L**, **Neumann D**, **Mihalef V**, **Meister F**, **Kramer M**, **Gulsun M**, **Kelm M**, **Kühne TCardioproof SharmaP.** Non-invasive assessment of patient-specific aortic haemodynamics from four- dimensional flow MRI data. *Interface Focus* 8: 20170006, 2018. doi:10.1098/rsfs.2017.0006.

9. **Westerhof BE**, **Westerhof N.** Magnitude and return time of the reflected wave: the effects of large artery stiffness and aortic geometry. *J Hypertens* 30: 932–939, 2012. doi:10.1097/HJH.0b013e3283524932.

10. **Guala A**, **Tosello F**, **Leone D**, **Sabia L**, **D'Ascenzo F**, **Moretti C**, **Bollati M**, **Veglio F**, **Ridolfi L**, **Milan A.** Multiscale mathematical

modeling vs. the generalized transfer function approach for aortic pressure estimation: a comparison with invasive data. *Hypertens Res* 42: 690–698, 2019. doi:10.1038/s41440-018-0159-5.

11. **Alastruey J**, **Xiao N**, **Fok H**, **Schaeffter T**, **Figueroa CA.** On the impact of modelling assumptions in multi-scale, subject-specific models of aortic haemodynamics. *J R Soc Interface* 13: 20160073, 2016. doi:10.1098/rsif.2016.0073.

12. **Bollache E**, **Kachenoura N**, **Redheuil A**, **Frouin F**, **Mousseaux E**, **Recho P**, **Lucor D.** Descending aorta subject-specific one-dimensional model validated against in vivo data. *J Biomech* 47: 424–431, 2014. doi:10.1016/j.jbiomech.2013.11.009.

13. **Delles M**, **Rengier F**, **Jeong Y-J**, **von Tengg-Kobligk H**, **Ley S**, **Kauczor H-U**, **Dillmann R**, **Unterhinninghofen R.** Estimation of aortic pressure waveforms from 4D phase-contrast MRI. *Annu Int Conf IEEE Eng Med Biol Soc.* 2013: 731–734, 2013. doi:10.1109/EMBC.2013.6609604.

14. **Khalifé M**, **Decoene A**, **Caetano F**, **de Rochefort L**, **Durand E**, **Rodríguez D.** Estimating absolute aortic pressure using MRI and a one-dimensional model. *J Biomech* 47: 3390–3399, 2014. doi:10.1016/j.jbiomech.2014.07.018.

15. **Frank O.** The basic shape of the arterial pulse. First treatise: mathematical analysis. 1899. *J Mol Cell Cardiol* 22: 255–277, 1990. doi:10.1016/0022-2828(90)91460-O.

16. **Westerhof N**, **Elzinga G**, **Sipkema P.** An artificial arterial system for pumping hearts. *J Appl Physiol* 31: 776–781, 1971. doi:10.1152/jappl.1971.31.5.776.

17. **Shi Y**, **Valverde I**, **Lawford PV**, **Beerbaum P**, **Hose DR.** Patient-specific non-invasive estimation of pressure gradient across aortic coarctation using magnetic resonance imaging. *J Cardiol* 73: 544–552, 2019. doi:10.1016/j.jjcc.2018.12.016.

18. **Li Y**, **Gu H**, **Fok H**, **Alastruey J**, **Chowienczyk P.** Forward and backward pressure waveform morphology in hypertension. *Hypertension* 69: 375–381, 2017. doi:10.1161/HYPERTENSIONAHA.116.08089.

19. **Sharman JE**, **Avolio AP**, **Baulmann J**, **Benetos A**, **Blacher J**, **Blizzard CL**, et al**.** Validation of non-invasive central blood pressure devices: ARTERY Society task force (abridged) consensus statement on protocol standardization. *Artery Res* 20: 35–43, 2017. doi:10.1016/j.artres.2017.11.001.

20. **Charlton PH**, **Mariscal Harana J**, **Vennin S**, **Li Y**, **Chowienczyk P**, **Alastruey J.** Modeling arterial pulse waves in healthy aging: a database for in silico evaluation of hemodynamics and pulse wave indexes. *Am J Physiol Heart Circ Physiol* 317: H1062–H1085, 2019. doi:10.1152/ajpheart.00218.2019.

21. **Charlton P**, **Mariscal Harana J**, **Vennin S**, **Li Y**, **Chowienczyk P**, **Alastruey J.** Pulse Wave Database (PWDB) algorithms. 2019. https://zenodo.org/record/3271513.

22. **Bos WJ**, **Verrij E**, **Vincent HH**, **Westerhof BE**, **Parati G**, **van Montfrans GA.** How to assess mean blood pressure properly at the brachial artery level. *J Hypertens* 25: 751–755, 2007. doi:10.1097/HJH.0b013e32803fb621.

23. **Dujardin JP**, **Stone DN.** Characteristic impedance of the proximal aorta determined in the time and frequency domain: a comparison. *Med Biol Eng Comput* 19: 565–568, 1981. doi:10.1007/BF02442770.

24. **Qureshi MU**, **Colebank MJ**, **Schreier DA**, **Tabima DM**, **Haider MA**, **Chesler NC**, **Olufsen MS.** Characteristic impedance: frequency or time domain approach? *Physiol Meas* 39: e014004, 2018. doi:10.1088/1361-6579/aa9d60.

25. **Stergiopulos N**, **Meister JJ**, **Westerhof N.** Simple and accurate way for estimating total and segmental arterial compliance: the pulse pressure method. *Ann Biomed Eng* 22: 392–397, 1994. doi:10.1007/BF02368245.

26. **Westerhof N**, **Lankhaar J-W**, **Westerhof BE.** The arterial Windkessel. *Med Biol Eng Comput* 47: 131–141, 2009. doi:10.1007/s11517-008-0359-2.

27. **Chemla D**, **Hébert JL**, **Coirault C**, **Zamani K**, **Suard I**, **Colin P**, **Lecarpentier Y.** Total arterial compliance estimated by stroke volume-to-aortic pulse pressure ratio in humans. *Am J Physiol* 274: H500–H505, 1998. doi:10.1152/ajpheart.1998.274.2.H500.

28. **Lucas CL**, **Wilcox BR**, **Ha B**, **Henry GW.** Comparison of time domain algorithms for estimating aortic characteristic impedance in humans. *IEEE Trans Biomed Eng* 35: 62–68, 1988. doi:10.1109/10.1337.

29. **Abel FL.** Fourier analysis of left ventricular performance. Evaluation of impedance matching. *Circ Res* 28: 119–135, 1971. doi:10.1161/01.RES.28.2.119.

30. **Alastruey J**, **Parker KH**, **Peiró J**, **Sherwin SJ.** Lumped parameter outflow models for 1-D blood flow simulations: effect on pulse waves and parameter estimation *Communications in Computational Physics* 4: 317–336, 2008. https://global-sci.org/intro/article_detail/cicp/7792.html.

31. **Bazett HC.** An analysis of the time-relations of electrocardiograms. *Ann Noninvasive Electrocardiol* 2: 177–194, 1997. doi:10.1111/j.1542-474X.1997.tb00325.x.

32. **Charlton PH**, **Celka P**, **Farukh B**, **Chowienczyk P**, **Alastruey J.** Assessing mental stress from the photoplethysmogram: a numerical study. *Physiol Meas* 39: 054001, 2018. doi:10.1088/1361-6579/aabe6a.

33. **Clarke TN**, **Prys-Roberts C**, **Biro G**, **Foex P**, **Bennet MJ.** Aortic input impedance and left ventricular energetics in acute isovolumic anaemia. *Cardiovasc Res* 12: 49–55, 1978. doi:10.1093/cvr/12.1.49.

34. **Davies JE**, **Whinnett ZI**, **Francis DP**, **Willson K**, **Foale RA**, **Malik IS**, **Hughes AD**, **Parker KH**, **Mayet J.** Use of simultaneous pressure and velocity measurements to estimate arterial wave speed at a single site in humans. *Am J Physiol Heart Circ Physiol* 290: H878–H885, 2006. doi:10.1152/ajpheart.00751.2005.

35. **Gaddum NR**, **Alastruey J**, **Beerbaum P**, **Chowienczyk P**, **Schaeffter T.** A technical assessment of pulse wave velocity algorithms applied to non-invasive arterial waveforms. *Ann Biomed Eng* 41: 2617–2629, 2013. doi:10.1007/s10439-013-0854-y.

36. **Hughes AD**, **Parker KH.** Forward and backward waves in the arterial system: impedance or wave intensity analysis? *Med Biol Eng Comput* 47: 207–210, 2009. doi:10.1007/s11517-009-0444-1.

37. **Kamoi S**, **Pretty C**, **Balmer J**, **Davidson S**, **Pironet A**, **Desaive T**, **Shaw GM**, **Chase JG.** Improved pressure contour analysis for estimating cardiac stroke volume using pulse wave velocity measurement. *BioMed Eng Online* 16: 51, 2017. doi:10.1186/s12938-017-0341-z.

38. **Mitchell GF**, **Pfeffer MA**, **Westerhof N**, **Pfeffer JM.** Measurement of aortic input impedance in rats. *Am J Physiol* 267: H1907–H1915, 1994. doi:10.1152/ajpheart.1994.267.5.H1907.

39. **Murgo JP**, **Westerhof N**, **Giolma JP**, **Altobelli SA.** Aortic input impedance in normal man: relationship to pressure wave forms. *Circulation* 62: 105–116, 1980. doi:10.1161/01.CIR.62.1.105.

40. **Nichols WW**, **Conti CR**, **Walker WE**, **Milnor WR.** Input impedance of the systemic circulation in man. *Circ Res* 40: 451–458, 1977. doi:10.1161/01.RES.40.5.451.

41. **Randall OS**, **Esler MD**, **Calfee RV**, **Bulloch GF**, **Maisel AS**, **Culp B.** Arterial compliance in hypertension. *Aust N Z J Med* 6: 49–59, 1976. doi:10.1111/j.1445-5994.1976.tb03323.x.

42. **Segers P**, **Verdonck P.** Role of tapering in aortic wave reflection: hydraulic and mathematical model study. *J Biomech* 33: 299–306, 2000. doi:10.1016/S0021-9290(99)00180-3.

43. **Self DA**, **Ewert DL**, **Swope RD**, **Crisman RP**, **Latham RD.** Beat-to-beat determination of peripheral resistance and arterial compliance during +Gz centrifugation. *Aviat Space Environ Med* 65: 396–403, 1994.

44. **Simon AC**, **Safar ME**, **Levenson JA**, **London GM**, **Levy BI**, **Chau NP.** An evaluation of large arteries compliance in man. *Am J Physiol* 237: H550–H554, 1979. doi:10.1152/ajpheart.1979.237.5.H550.

45. **Tabima DM**, **Roldan-Alzate A**, **Wang Z**, **Hacker TA**, **Molthen RC**, **Chesler NC.** Persistent vascular collagen accumulation alters hemodynamic recovery from chronic hypoxia. *J. Biomech* 45: 799–804, 2012. doi:10.1016/j.jbiomech.2011.11.020.

46. **Westerhof N**, **Elzinga G.** Normalized input impedance and arterial decay time over heart period are independent of animal size. *Am J Physiol* 261: R126–R133, 1991. doi:10.1152/ajpregu.1991.261.1.R126.

47. **Westerhof N**, **Bosman F**, **De Vries CJ**, **Noordergraaf A.** Analog studies of the human systemic arterial tree. *J Biomech* 2: 121–143, 1969. doi:10.1016/0021-9290(69)90024-4.

48. **Bland JM**, **Altman DG.** Statistical methods for assessing agreement between two methods of clinical measurement. *Lancet* 1: 307–310, 1986. doi:10.1016/S0140-6736(86)90837-8.

49. **Hickson SS**, **Butlin M**, **Graves M**, **Taviani V**, **Avolio AP**, **McEniery CM**, **Wilkinson IB.** The relationship of age with regional aortic stiffness and diameter. *JACC Cardiovasc Imaging* 3: 1247–1255, 2010. doi:10.1016/j.jcmg.2010.09.016.

50. **Liang YL**, **Teede H**, **Kotsopoulos D**, **Shiel L**, **Cameron JD**, **Dart AM**, **McGrath BP.** Non-invasive measurements of arterial structure and function: repeatability, interrelationships and trial sample size. *Clin Sci* 95: 669–679, 1998. doi:10.1042/cs0950669.

51. **Parazynski SE**, **Tucker BJ**, **Aratow M**, **Crenshaw A**, **Hargens AR.** Direct measurement of capillary blood pressure in the human lip. *J Appl Physiol (1985)* 74: 946–950, 1993. doi:10.1152/jappl.1993.74.2.946.

52. **Weissler AM**, **Peeler RG**, **Roehll WH Jr.** Relationships between left ventricular ejection time, stroke volume, and heart rate in normal individuals and patients with cardiovascular disease**.** *Am Heart J* 62: 367–378, 1961. doi:10.1016/0002-8703(61)90403-3.

53. **Florkow M**, **Mariscal Harana J**, **van Engelen A**, **Schneider T**, **Rafiq I**, **de Bliek H**, **Alastruey J**, **Botnar R.** An integrated software application for non-invasive assessment of local aortic haemodynamic parameters. *Procedia Comput Sci* 90: 2–8, 2016. doi:10.1016/j.procs.2016.07.002.

54. **Oliván Bescós J**, **Sonnemans J**, **Habets R**, **Peters J**, **van den Bosch H**, **Leiner T.** Vessel explorer: a tool for quantitative measurements in CT and MR angiography. *MedicaMundi* 53: 64–71, 2009. https://www.semanticscholar.org/paper/Vessel-Explorer-%3A-a-tool-for-quantitative-in-CT-and-Bescós-Sonnemans/1d1107ac4d35819bd61f9a82153b6ed97a692996.

55. **Hassan S**, **Turner P.** Systolic time intervals: a review of the method in the non-invasive investigation of cardiac function in health, disease and clinical pharmacology. *Postgrad Med J*. 59: 423–434, 1983. doi:10.1136/pgmj.59.693.423.

56. **Parragh S**, **Hametner B**, **Wassertheurer S.** Influence of an asymptotic pressure level on the windkessel models of the arterial system. *IFAC-PapersOnLine* 48: 17–22, 2015. doi:10.1016/j.ifacol.2015.05.125.

57. **Vermeersch SJ**, **Rietzschel ER**, **De Buyzere ML**, **Van Bortel LM**, **Gillebert TC**, **Verdonck PR**, **Segers P.** The reservoir pressure concept: the 3-element windkessel model revisited? Application to the Asklepios population study. *J Eng Math* 64: 417–428, 2009. doi:10.1007/s10665-009-9286-y.

58. **Aguado-Sierra J**, **Alastruey J**, **Wang J-J**, **Hadjiloizou N**, **Davies J**, **Parker KH.** Separation of the reservoir and wave pressure and velocity from measurements at an arbitrary location in arteries. *Proc Inst Mech Eng H* 222: 403–416, 2008. doi:10.1243/09544119JEIM315.

59. **Caldini P**, **Permutt S**, **Waddell JA**, **Riley RL.** Effect of epinephrine on pressure, flow, and volume relationships in the systemic circulation of dogs. *Circ Res* 34: 606–623, 1974. doi:10.1161/01.RES.34.5.606.

60. **Wang J-J**, **Flewitt JA**, **Shrive NG**, **Parker KH**, **Tyberg JV.** Systemic venous circulation. Waves propagating on a windkessel: relation of arterial and venous windkessels to systemic vascular resistance. *Am J Physiol Heart Circ Physiol* 290: H154–H162, 2006. doi:10.1152/ajpheart.00494.2005.

61. **Ohno Y Kanno  YTakenaka T.** Central blood pressure and chronic kidney disease. *World J Nephrol* 5: 90-100, 2016. doi:10.5527/wjn.v5.i1.90.

62. **O'Rourke MF.** Arterial aging: pathophysiological principles. *Vasc Med* 12: 329–341, 2007. doi:10.1177/1358863X07083392.

63. **Randall OS**, **van den Bos GC**, **Westerhof N.** Systemic compliance: does it play a role in the genesis of essential hypertension? *Cardiovasc Res* 18: 455–462, 1984. doi:10.1093/cvr/18.8.455.

64. **Stergiopulos N**, **Meister JJ**, **Westerhof N.** Evaluation of methods for estimation of total arterial compliance. *Am J Physiol* 268: H1540–1548, 1995. doi:10.1152/ajpheart.1995.268.4.H1540.

65. **Bailey MA**, **Davies JM**, **Griffin KJ**, **Bridge KI**, **Johnson AB**, **Sohrabi S**, **Baxter PD**, **Scott DJ.** Carotid-femoral pulse wave velocity is negatively correlated with aortic diameter. *Hypertens Res* 37: 926–932, 2014. doi:10.1038/hr.2014.101.

66. **Reference Values for Arterial Stiffness' Collaboration.** Determinants of pulse wave velocity in healthy people and in the presence of cardiovascular risk factors: 'establishing normal and reference values'. *Eur Heart J* 31: 2338–2350, 2010. doi:10.1093/eurheartj/ehq165.

67. **Obeid H**, **Soulat G**, **Mousseaux E**, **Laurent S**, **Stergiopulos N**, **Boutouyrie P**, **Segers P.** Numerical assessment and comparison of pulse wave velocity methods aiming at measuring aortic stiffness. *Physiol Meas* 38: 1953–1967, 2017. doi:10.1088/1361-6579/aa905a.

68. **Vennin S**, **Li Y**, **Willemet M**, **Fok H**, **Gu H**, **Charlton P**, **Alastruey J**, **Chowienczyk P.** Identifying hemodynamic determinants of pulse pressure: a combined numerical and physiological approach. *Hypertension* 70: 1176–1182, 2017. doi:10.1161/HYPERTENSIONAHA.117.09706.

69. **Khir AW**, **O'Brien A**, **Gibbs JS**, **Parker KH.** Determination of wave speed and wave separation in the arteries. *J Biomech* 34: 1145–1155, 2001. doi:10.1016/S0021-9290(01)00076-8.

70. **Epstein S**, **Willemet M**, **Chowienczyk PJ**, **Alastruey J.** Reducing the number of parameters in 1D arterial blood flow modeling: less is more for patient-specific simulations. *Am J Physiol Heart Circ Physiol* 309: H222–H234, 2015. doi:10.1152/ajpheart.00857.2014.

71. **Fossan FE**, **Mariscal Harana J**, **Alastruey J**, **Hellevik LR.** Optimization of topological complexity for one-dimensional arterial blood flow models. *J R Soc Interface* 15: 20180546, 2018. doi:10.1098/rsif.2018.0546.

72. **Fok H**, **Guilcher A**, **Brett S**, **Jiang B**, **Li Y**, **Epstein S**, **Alastruey J**, **Clapp B**, **Chowienczyk P.** Dominance of the forward compression wave in determining pulsatile components of blood pressure: similarities between inotropic stimulation and essential hypertension. *Hypertension* 64: 1116–1123, 2014. doi:10.1161/HYPERTENSIONAHA.114.04050.

73. **Papaioannou TG**, **Karageorgopoulou TD**, **Sergentanis TN**, **Protogerou AD**, **Psaltopoulou T**, **Sharman JE**, **Weber T**, **Blacher J**, **Daskalopoulou SS**, **Wassertheurer S**, **Khir AW**, **Vlachopoulos C**, **Stergiopulos N**, **Stefanadis C**, **Nichols WW**, **Tousoulis D.** Accuracy of commercial devices and methods for noninvasive estimation of aortic systolic blood pressure a systematic review and meta-analysis of invasive validation studies. *J Hypertens* 34: 1237–1248, 2016. doi:10.1097/HJH.0000000000000921.